CHAPTER 5

THEORETICAL INSIGHT ON ATMOSPHERIC CHEMISTRY OF HFE-365MCF3 AND HFE-7000 (i-$C_3F_7OCH_3$)

In this chapter, we have investigated the atmospheric chemistry of two different HFEs. The chapter contains two sections.

In **section 5.1**, the mechanism and kinetics of the gas-phase reactions of $CF_3CF_2CH_2OCH_3$ (HFE-365mcf3) with the OH radicals have been performed using meta-hybrid modern density functional M06-2X in conjunction of 6-31+G(d,p) basis set. Reaction profiles for OH-initiated hydrogen abstraction are modeled including the formation of pre-reactive and post-reactive complexes at entrance and exit channels. Our calculations reveal that hydrogen abstraction from the $–CH_2$ group is thermodynamically more facile than that from the $–CH_3$ group. This is further ascertained by the calculated C-H bond dissociation energy of $CF_3CF_2CH_2OCH_3$ molecule. The rate constants of the titled reactions are computed over the temperature range of 250–450 K. The atmospheric life time of HFE-365mcf3 is estimated to be 42 days. The atmospheric fate of the alkoxy radicals, $CF_3CF_2CH(O^{\bullet})OCH_3$ and $CF_3CF_2CH_2OCH_2O^{\bullet}$ are also investigated for the first time using the same level of theory [Bhattacharjee, D., Mishra, B. K. and Deka, R. C. Theoretical insight on atmospheric chemistry of HFE-365mcf3: reactions with OH radicals, atmospheric lifetime, and fate of alkoxy radicals ($CF_3CF_2CH(O^{\bullet})$ OCH_3/$CF_3CF_2CH_2OCH_2O^{\bullet}$). *Journal of molecular modeling*, 21:69, 2015].

In section **5.2,** we have studied the mechanism of the hydrogen abstraction reaction between HFE-7000 (i-$C_3F_7OCH_3$) and the OH radicals using M06-2X functional with 6-31+G(d,p) basis set. The pre-reactive and post-reactive complexes from intrinsic reaction coordinate calculations are validated at entrance and exit channels, respectively. The standard enthalpies of formation for species and bond dissociation energy for C-H bond are also reported. The rate constants of the titled reactions are computed over the temperature range of 250–450 K. The atmospheric life time of i-HFE-7000 is estimated to be 3.10 years. The atmospheric fate of the alkoxy radical, (i-$C_3F_7OCH_2O^{\bullet}$) is also explored for the first time using same level of theory. First theoretical rate constant for the OH-initiated hydrogen abstraction of isofluoro-propyl formate (i- $C_3F_7OC(O)H$) is also reported [Mishra, B. K., Gour, N. K., Bhattacharjee, D. and Deka, R. C. Atmospheric chemistry of HFE-7000 (i-$C_3F_7OCH_3$) and isofluoro-propyl formate (i-C_3F_7OC (O)H): reactions with OH radicals, atmospheric lifetime and fate of alkoxy radical (i-$C_3F_7OCH_2O$•)–a DFT study. *Molecular Physics*, 114:618-626, 2016].

5.1 ATMOSPHERIC CHEMISTRY OF HFE-365MCF3

5.1.1 INTRODUCTION

In recent times, hydrofluoroethers (HFEs) are proposed as a third generation substitute for CFCs, HFCs and HCFCs in industries as well as solvent in laboratories. [1,2]. They do not contain harmful chlorine and bromine atoms that cause the ozone layer depletion [3]. The lifetime of HFEs are relatively small as predicted from their rate constant with OH initiated reactions and thus they have less threatening to global warming. [4]. The primary product of the oxidation of HFEs produce fluorinated esters (FESs) which further undergo hydrolysis to produce environmentally burdened product such as trifluoroacetic acid (TFA) and COF_2 [5-7]. It is very obvious and necessary to understand of the atmospheric chemistry of these compounds.

Two experimental studies are reported for the H-abstraction reaction from $CF_3CF_2CH_2OCH_3$ with OH by Oyaro *et al.* [8] and Thomsen *et al.* [9].

$$CF_3CF_2CH_2OCH_3 + OH \longrightarrow CF_3CF_2C^{\bullet}HOCH_3 + H_2O \quad (5.1.1)$$

$$CF_3CF_2CH_2OCH_3 + OH \longrightarrow CF_3CF_2CH_2OC^{\bullet}H_2 + H_2O \quad (5.1.2a\&\ 5.1.2b)$$

First experimental studies of the above reactions was carried out by Oyaro *et al.* [8] using a relative rate method and the experimental overall rate constant was found to be (6.42±0.33) × 10-13 cm^3 $molecule^{-1}$ s^{-1} at 298 K. Thomsen *et al.* [9] performed further experimental study with the help of FTIR smog chamber technique and reported a rate constants value as k(OH + CF3CF2CH2OCH3) = (5.78±1.02)×10-13 cm^3 $molecule^{-1}$ s^{-1} at 296±1 K. These two experimental studies are in close agreement with the rate constant value as (3.93×10-13 cm^3 $molecule^{-1}$ s^{-1}) which was estimated empirically by Urata *et al.* [10] on the basis of bond dissociation enthalpies (BDE's) of the C–H bond by using the artificial neural network (ANN) technique. Moreover, experimental studies provided only the total rate constant and it is difficult to predict the detailed mechanism and thermo chemistry. Thus, for better understanding of mechanistic pathways, kinetics and thermochemistry we must rely on quantum chemical methods.

In present work, for the first time we have studied the mechanism and kinetics of H-abstraction reaction from $CF_3CF_2CH_2OCH_3$ with OH radicals using DFT

methods. Our calculation suggests that one reaction channel each from $–CH_2$ group and two transition states from $–CH_3$ group are feasible for the $CF_3CF_2CH_2OCH_3$ + OH reactions as given in reactions (5.1.1-5.1.2).

The tropospheric degradation of $CF_3CF_2CH_2OCH_3$ is initiated by attack of OH radicals which leads to the formation of alkyl radical $CF_3CF_2C^{\bullet}HOCH_3$. The latter reacts with atmospheric O_2 to produce peroxy radical, $CF_3CF_2CH(OO^{\bullet})OCH_3$. In a polluted atmosphere, the peroxy radical thus formed may further reacts with other oxidizing species such as NO_2 and NO that ultimately leads to the formation of alkoxy radical $CF_3CF_2CH(O^{\bullet})OCH_3$. On the other hand, alkoxy radical, $CF_3CF_2CH_2OCH_2O^{\bullet}$ may also be generated through hydrogen abstraction from the $-CH_3$ group. The chemistry of alkoxy radicals, thus generated has been a subject of extensive experimental and theoretical investigations because they are interesting intermediates in the atmospheric oxidation of volatile organic compounds. The report of Oyaro *et al.* [8] reveals that that C-C bond scission leading to $CF_3C^{\bullet}F_2$ and methyl formate (CH_3OCHO) is not an important atmospheric sink for the consumption of $CF_3CF_2CH(O^{\bullet})OCH_3$ radical. The study of Thomsen *et al.* [9] concluded that the atmospheric fate of $CF_3CF_2CH(O^{\bullet})OCH_3$ radical is C-C bond scission. Due to this discrepancy, there is a need to perform quantum mechanical calculations to determine the energetics involved during the decomposition of $CF_3CF_2CH(O^{\bullet})OCH_3$ radical. Till date, no theoretical study has been performed to elucidate the dissociative pathways of alkoxy radicals. This motivated us to theoretically investigate the decomposition and reactivity mechanism.

There are two potential pathways for decomposition of alkoxy radicals produced from $CF_3CF_2CH_2OCH_3$ that involve bond scissions and oxidation processes. These are represented as follows:

$$CF_3CF_2CH(O^{\bullet})\,OCH_3 \longrightarrow CF_3C^{\bullet}F_2 + CH_3OC(O)H \qquad (5.1.3)$$

$$\longrightarrow CF_3CF_2C(O^{\bullet})CH_3 + H \qquad (5.1.4)$$

$$+ O_2 \longrightarrow CF_3CF_2C(O^{\bullet})CH_3 + HO^{\bullet}_2 \qquad (5.1.4)$$

$$CF_3CF_2CH_2OCH_2O^{\bullet} \longrightarrow CF_3CF_2CH_2OCHO + H \qquad (5.1.6)$$

$$+ O_2 \longrightarrow CF_3CF_2CH_2OCHO + HO^{\bullet}_2 \qquad (5.1.7)$$

Bond dissociation energies (BDEs) of the breaking C-H bonds are known to be strongly correlated with the observed reactivity trend for the hydrogen abstraction reaction, and the ether linkage (-O-) is important for the reactivity of the hydrofluoroethers [11,12]. Thus, we present BDE of the two types of C-H bonds in $CF_3CF_2CH_2OCH_3$. In addition, the knowledge of accurate enthalpy of formation ($\Delta_fH°_{298}$) for $CF_3CF_2CH_2OCH_3$, $CF_3CF_2C^{\bullet}HOCH_3$ and $CF_3CF_2CH_2OC^{\bullet}H_2$ radicals is of vital importance for determining the thermodynamic properties and atmospheric modeling. Thus we also predict the enthalpies of formation using isodesmic reactions at M06-2X/6-31+G(d,p) level.

5.1.2 COMPUTATIONAL DETAILS

We have carried out all the calculations performed here with the Gaussian 09 suite of program [13]. Geometry optimizations are made at the M06-2X level [14] of theory using 6-31+G(d,p) basis set. The 6-31+G(d,p) basis set are used because the same basis set was used for developing the model functional. M06-2X hybrid density functional already provides reliable results for thermo chemistry and kinetics of the previous works [15-19]. It is a hybrid meta-DFT method with a high percentage of HF exchange, and it has broadest applicability with average mean absolute errors of about 1.3, 1.2, and 0.5 kcal mol^{-1} for thermochemical, barrier height and non-covalent interaction calculations, respectively [20]. Due to the formation of pre- and post-reaction complex, the shape of potential energy surface for the hydrogen abstraction reactions by OH radicals modifies and hence it affects the tunneling factor [21,22]. As a result the rate constant for hydrogen abstraction also changes. Therefore, we also validated pre- and post reactive complexes along the entry and exit of the reaction path. In order to determine the nature of different stationary points on the potential energy surface, vibrational frequencies calculations are performed using the same level of theory at which the optimization was made. Further, to ascertain that the identified transition states connect reactant and products smoothly, intrinsic reaction coordinate (IRC) calculations [23] are also performed at the M06-2X/6-31+G(d,p) level.

5.1.3 RESULTS AND DISCUSSION

5.1.3.1 Structure and energetics

The calculated enthalpy of reactions ($\Delta_rH°_{298}$) and reaction free energies ($\Delta_rG°_{298}$) at 298 K for the reactions of $CF_3CF_2CH_2OCH_3$ with OH radicals are recorded in Table 5.1.1. The table indicates that the enthalpy of reaction, ($\Delta_rH_{298}°$) values given in for 5.1.1 and 5.1.2 of both the reactions are significantly exothermic and exergonic in nature and thus thermodynamically feasible. There are two potential hydrogen abstraction sites of $CF_3CF_2CH_2OCH_3$, namely the $–CH_2$ and $–CH_3$ group. It can be seen from the geometrical parameters and stereographical orientation that the hydrogen atoms in the $–CH_3$ groups are not equivalent. Two transition states (TS2a and TS2b) are therefore located for $CF_3CF_2CH_2OCH_3$ + OH reactions from the $–CH_3$ group. Optimized geometries of reactants and transition states obtained at the M06-2X/6-31+G(d,p) level are shown in Figure 5.1.1. The reactant complexes, product complexes and products are depicted in Figure 5.1.2.

Table 5.1.1 Reaction enthalpies, free energies of reactions (5.1-5.2) and bond dissociation energy (D^0_{298}) calculated at M06-2X/6-31+G(d,p) level of theory along with literature values. All values are in kcal mol^{-1}.

Reaction Channels	**$\Delta_rH°_{298}$**	**$\Delta_rG°_{298}$**
Reaction 5.1.1	-22.09	-23.56
Reaction 5.1.2	-18.52	-19.15
Bond dissociation type	**M06-2X/ 6-31+G(d,p)**	**Liter. value[a]**
$CF_3CF_2CH_2OCH_3 \longrightarrow CF_3CF_2C^{\bullet}HOCH_3 + H$	96.78	94.59
$CF_3CF_2CH_2OCH_3 \longrightarrow CF_3CF_2CH_2OC^{\bullet}H_2 + H$	100.35	97.15

[a] Ref. [10]

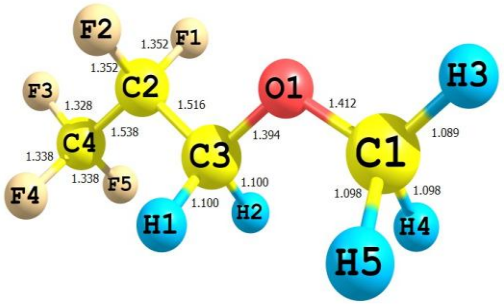

$CF_3CF_2CH_2OCH$

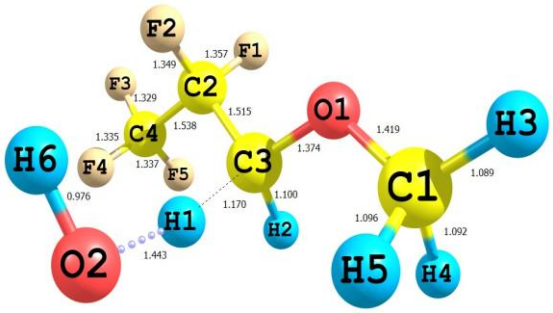

TS1

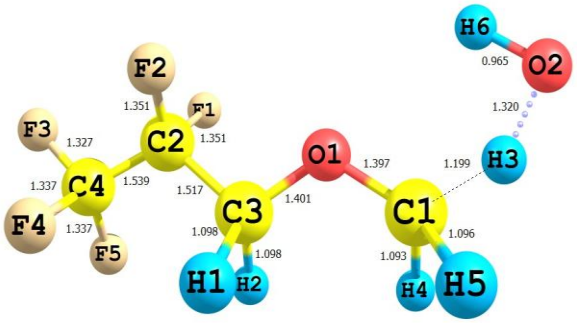

TS2a

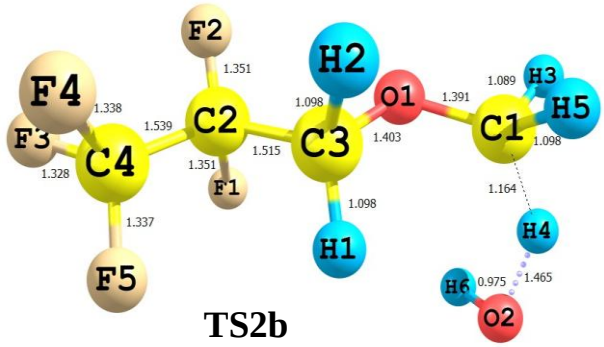

TS2b

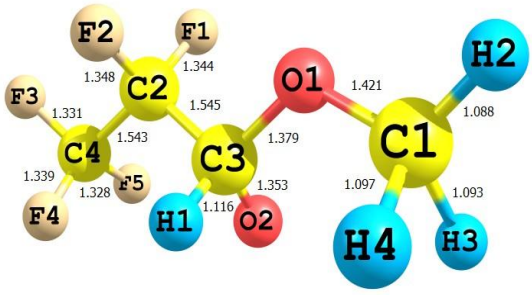

$CF_3CF_2CH(O^{\bullet})OCH_3$

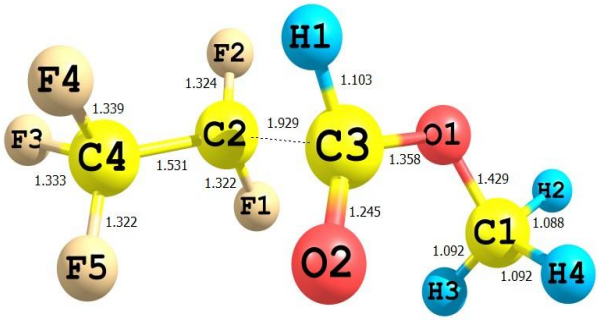

TS3

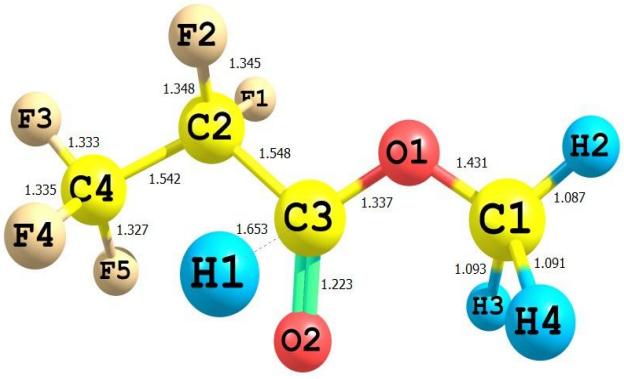

TS4

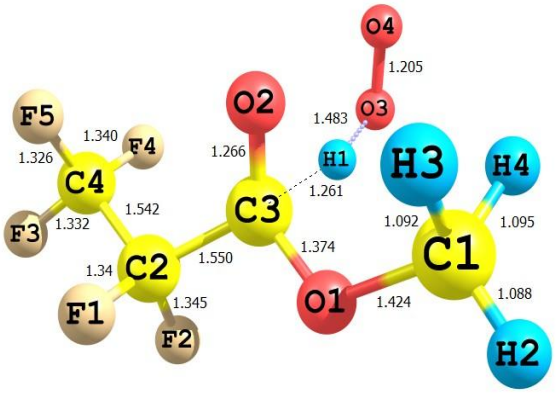

TS5

Continue…..

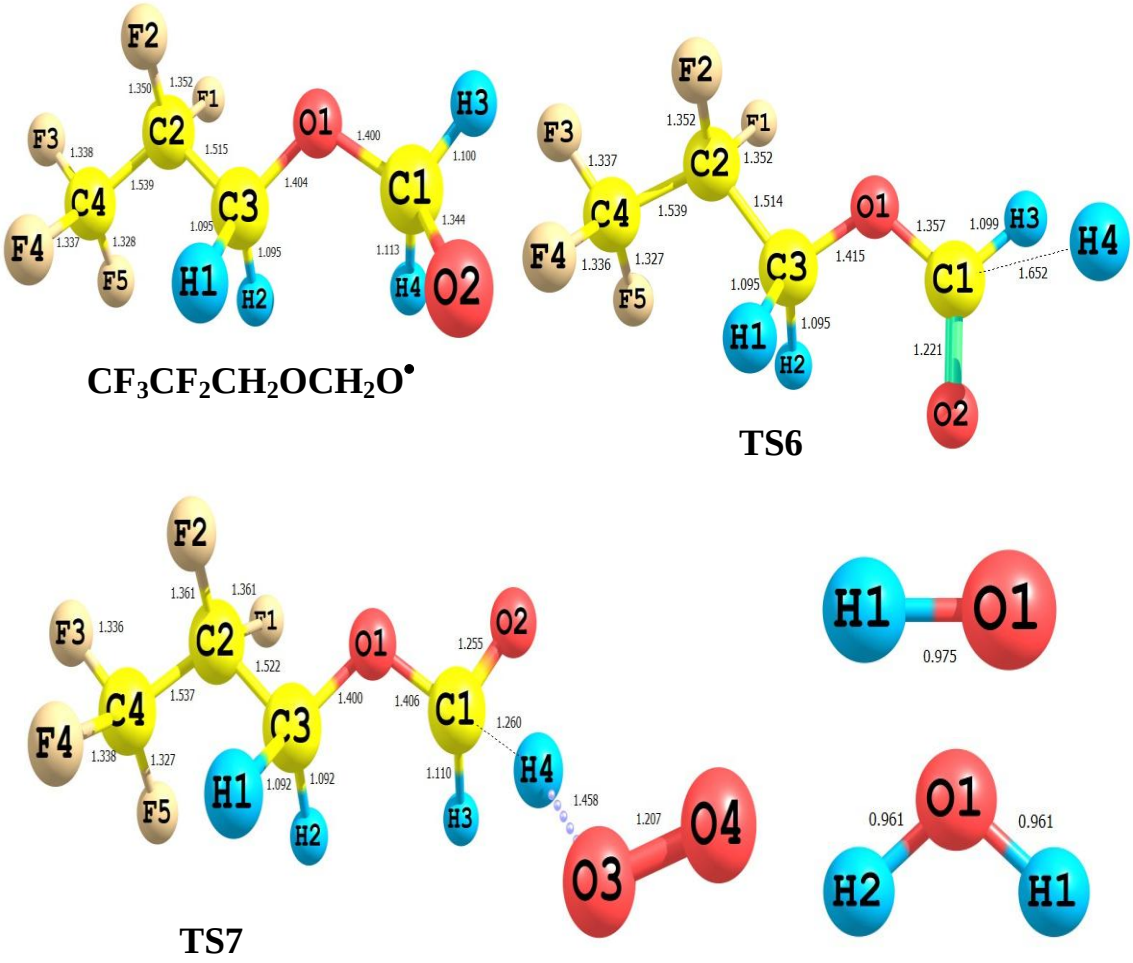

Figure 5.1.1 Optimized geometries of reactants and transition states at M06-2X/6-31+G(d,p) level. Bond lengths are in Angstroms.

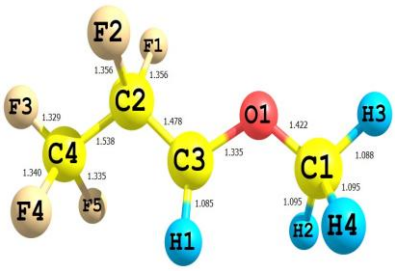

$CF_3CF_2CHOCH_3$

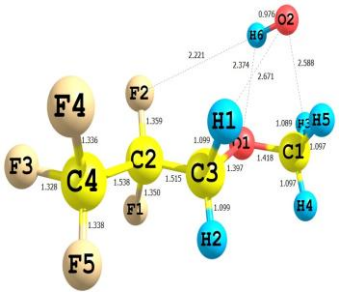

RC1/RC2b

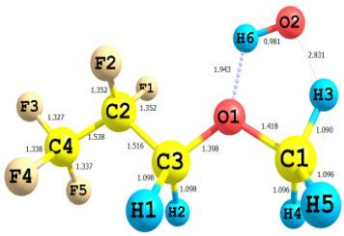

RC2a

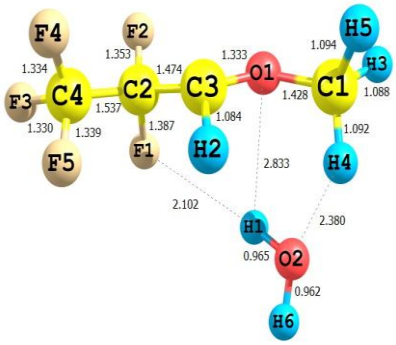

PC1

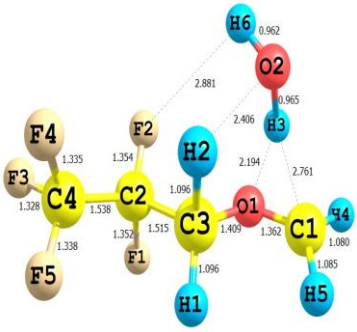

PC2a

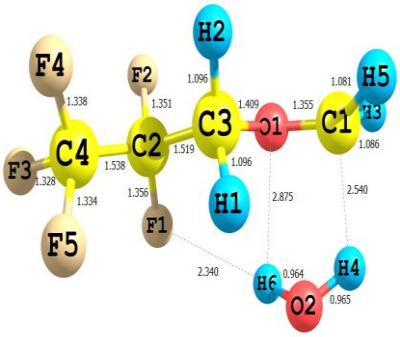

PC2b

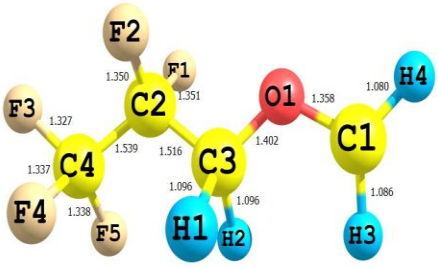

$CF_3CF_2CH_2OCH_2$

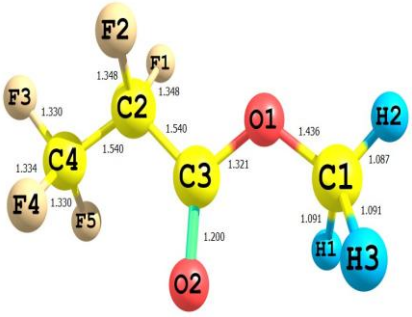

$CF_3CF_2C(O)OCH_3$

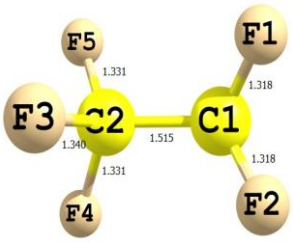

CF_3CF_2

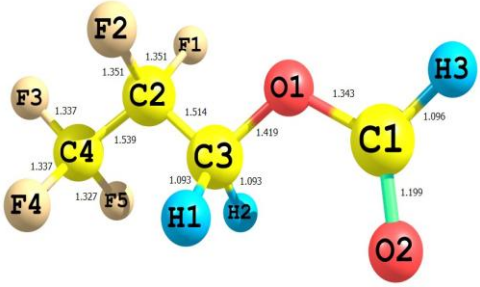

$CF_3CF_2CH_2OC(O)H$

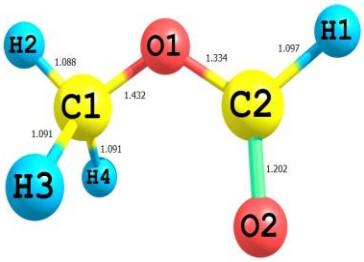

$CH_3OC(O)H$

Figure 5.1.2 Optimized geometries of reactant complexes, product complexes and products at M06-2X/6-31+G(d,p) level. Bond lengths are in Angstroms.

In the entrance channel for reactions of hydrogen abstraction by OH radicals (5.1.1 and 5.1.2a), pre- reactive complexes (RC1 and RC2a) have been located in the present work. However, for reaction channels 5.1.1 and 5.1.2b, we have obtained the same pre- reactive complexes (RC1/RC2b). In the exit channels also, there are product complexes occurring before the release of the final products and are labeled as PC1, PC2a and PC2b. In pre-reactive complex RC1, four hydrogen bonds are formed between the O1…H6, O2…H1, O2…H3 and F2…H6 bonds with the bond distances of 2.374, 2.671, 2.588 and 2.221 Å, respectively. However, in the complex RC2a, the two hydrogen bonds are formed between the O1…H6, and O2…H3 bonds with the bond distances of 1.943 and 2.831 Å, respectively. The other bond lengths are very close to those in equilibrium structures of $CF_3CF_2CH_2OCH_3$ molecule. At the same time, the post-reaction hydrogen bonded complexes (PC1, PC2a and PC2b) with energy less than the corresponding products are located at the exits of the reaction channels 5.1.1 and 5.1.2 for reactions with OH radicals which can be identified with relatively strong C–H…O and O-H…F bonds, as shown in Figure 5.1.2. Thus it is clear that the reaction channels 5.1.1 and 5.1.2 may proceed via indirect mechanisms. During the formation of transition states, the important structural parameters need to be observed are one of the C-H bond of the leaving hydrogen and the newly formed bond between H and O atoms in the OH radical. Visualization of the optimized structure of TS1, TS2a and TS2b further reveals that the breaking C-H bond is found to be longer in a range of 6.01–10.10% than the observed C-H bond length in isolated $CF_3CF_2CH_2OCH_3$; whereas the forming O...H bond length is longer by 37.35-52.44% than the O-H bond length in H_2O. The fact that the elongation of forming bond is larger than that of the breaking bond indicates that the barrier of the reactions (5.1.1-5.1.2) is near the corresponding reactants. This means the reaction will proceeds via early transition state structure which is in consonance with Hammond's postulate [24] that applicable to an exothermic hydrogen abstraction channel.

The frequency calculation results for species in reactions (5.1.1-5.1.2) are provided in Table B.1 of Appendix B. These results show that the reactants, intermediates and products possess stable minima on the potential energy surface which are identified by the presence of only real vibrational frequencies. The transition

states are characterized by only one imaginary frequency at 944i, 1334i and 868i cm-1 for TS1, TS2a and TS2b, respectively. The validity of transition state on the potential energy surface is confirmed by intrinsic reaction coordinate (IRC) calculation at the same level of theory. The zero point corrected relative energies for all the species present in reaction channels (5.1.1-5.1.2) are recorded in Table 5.1.2 at M06-2X/6-31+G(d,p) level of theory. From the table 5.1.2, we found that energy barriers for H-abstraction reaction channels from the $–CH_2$ and $–CH_3$ groups are -0.21, 2.68 and 0.14 kcal mol^{-1} for TS1, TS2a and TS2b, respectively.

Table 5.1.2 Zero point corrected relative energies (in kcal mol^{-1}) for all the species M06-2X/6-31+G(d,p) level of theory.

Species	**Relative energy (kcal mol^{-1})**
R + OH	0.00
RC1	-5.72
RC2a	-4.78
RC2b	-5.72
TS1	-0.21
TS2a	2.68
TS2b	0.14
PC1	-27.85
PC2a	-23.27
PC2b	-22.91
P1 + H_2O	-22.52
P2 + H_2O	-18.72

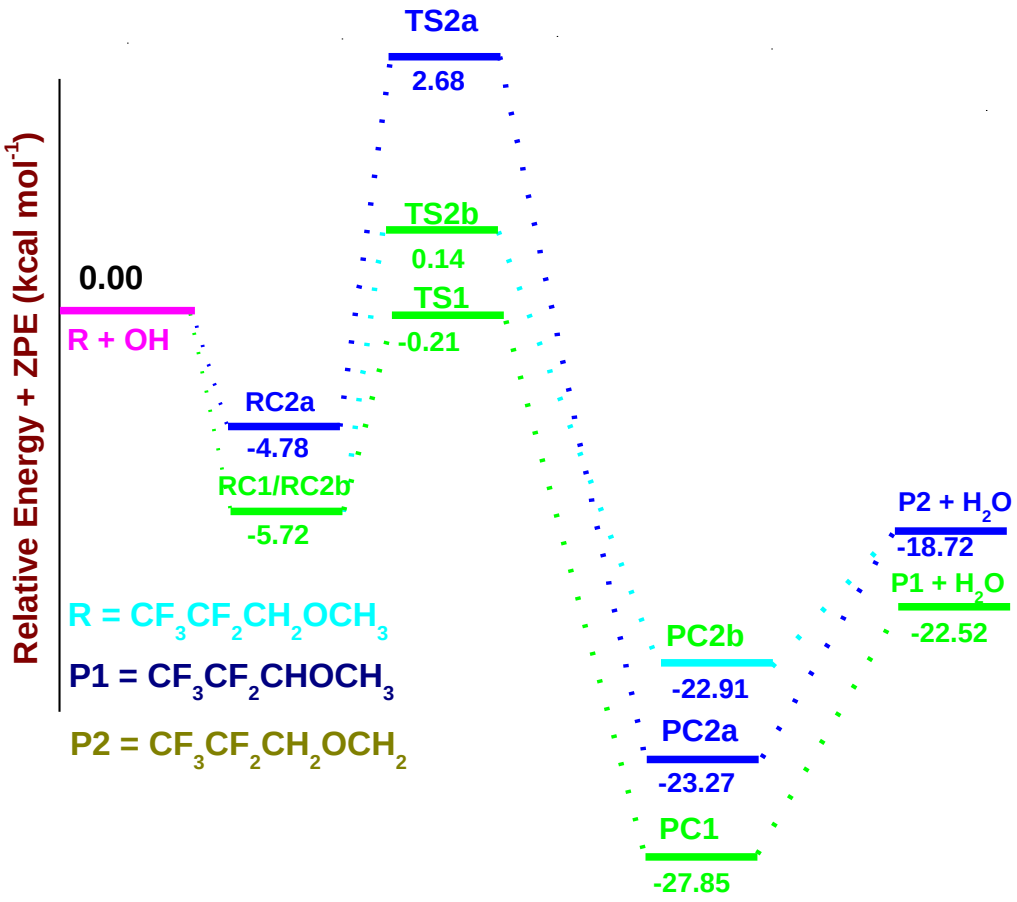

Figure 5.1.3 Potential energy profile for the $CF_3CF_2CH_2OCH_3$ + OH reactions. Relative energies (in kcal mol^{-1}) at M06-2X/6-31+G(d,p) level.

The energy profile diagram for the title reaction is also generated and provided in Figure 5.1.3. During construction of energy diagram, zero-point energy corrected total energy data as recorded in Table 5.1.2 are utilized. These energies are plotted with respect to the ground state energy of $CF_3CF_2CH_2OCH_3$ + OH including ZPE arbitrarily taken as zero. Here, spin contamination is not an issue for the $CF_3CF_2CH_2OCH_3$ + OH reactions because $<S^2>$ is found to be 0.76 at M06-2X/6-31+G(d, p) before annihilation which is only slightly greater than the expected value of $<S^2>$= 0.75 for doublets. The barrier height values suggest that OH-initiated hydrogen abstraction from the $–CH_2$ group of $CF_3CF_2CH_2OCH_3$ is more feasible than that from the $–CH_3$ group. However, this results contradicts with the observation of Thomsen *et al.* [9] that hydrogen abstraction by OH radicals proceeds 44±5% from the $–CH_2$ group and 56±5% from the

$-CH_3$ group. Our result is further confirmed by C-H bond dissociation energies calculations. The determined bond-dissociation energies, BDE (D^0_{298}) of the C-H bonds of $CF_3CF_2CH_2OCH_3$ molecule at M06-2X/6-31+G(d,p) are recorded in Table 5.1.1 along with literature values. The D^0_{298} value for C–H bonds in the $-CH_2$ and $-CH_3$ sites of $CF_3CF_2CH_2OCH_3$ amount to be 96.78 and 100.35 kcal mol^{-1}, respectively. Our presented BDE values for the C–H bonds agree well with the theoretical values of 94.59 and 97.15 kcal mol^{-1}, respectively for $-CH_2$ and $-CH_3$ sites of $CF_3CF_2CH_2OCH_3$ reported by Urata *et al.* [10] using ANN technique. It has been established that this functional (M06-2X) was better in computing the bond dissociation enthalpies [25,26].

The standard enthalpy of formation ($\Delta_fH°_{298}$) for $CF_3CF_2CH_2OCH_3$ and generated product radical i.e.; $CF_3CF_2C^{\bullet}HOCH_3$ (P1) and $CF_3CF_2CH_2OC^{\bullet}H_2$ (P2) would be valuable information for the further studies. However, these values are yet to be reported. The group-balanced isodesmic reactions are used here to calculate the $\Delta_fH°_{298}$. In these reactions, the number and types of bonds are remaining same. We have proposed three isodesmic reactions to estimate the enthalpies of formation of $CF_3CF_2CH_2OCH_3$. These are given below:

$$CF_3CF_2CH_2OCH_3 + CH_3F \longrightarrow CH_3OCH_3 + CF_3CH_2CF_3 \quad (5.1.8)$$

$$CF_3CF_2CH_2OCH_3 + CHF_3 \longrightarrow CF_3CH_2OCHF_2 + CH_3CF_3 \quad (5.1.9)$$

$$CF_3CF_2CH_2OCH_3 + CH_2F_2 + CF_3 \longrightarrow CHF_2OCHF_2 + CF_3CH_2CF_3 + CH_3 \quad (5.1.10)$$

The structures of all the species taking part in the reactions (5.1.8-5.1.10) are optimized at M06-2X/6-31+G(d,p) level. The $\Delta_fH°_{298}$ values for CH_3F: -55.62 kcal mol^{-1}, CH_2F_2: - 107.77 kcal mol^{-1} , CHF_3: -166.08 kcal mol^{-1}, CH_3: 34.82 kcal mol^{-1} and CF_3: -111.75 kcal mol^{-1} are taken from the work of Csontos *et al.* [27], where as for CH_3OCH_3: -44.0 kcal mol^{-1}, $CF_3CH_2OCHF_2$: -319.38 kcal mol^{-1}, $CF_3CH_2CF_3$: -336.5 kcal mol^{-1}, CH_3CF_3: -178.94 kcal mol^{-1}, CH_3CH_3: -20.24 kcal mol^{-1} and CHF_2OCHF_2: -259.1 kcal mol^{-1} are taken from the report of Kondo *et al.* [28] to evaluate the required enthalpies of formation. The calculated values of enthalpies of formation are listed in Table 5.1.3. As from the table, the values of $\Delta_fH°_{298}$ for the species obtained by the three working chemical reactions are consistent with each

other. The average $\Delta_fH°_{298}$ for $CF_3CF_2CH_2OCH_3$ calculated from M06-2X/6-31+G(d,p) result is found to be -307.89 kcal mol^{-1}. It is seen that the calculated $\Delta_fH°_{298}$ for $CF_3CF_2CH_2OCH_3$ at M06-2X/6-31+G(d,p) method is found to be in good agreement with a theoretical value of -309.27 kcal mol^{-1} reported by Kondo *et al.* [28] . in which they used bond additivity corrected MP2 method (BAC-MP2/6-31G**) as well as atom additivity corrected MP2 method (AAC-MP2/6-31G**). The $\Delta_fH°_{298}$ values for $CF_3CF_2C^{\bullet}HOCH_3$ (P1) and $CF_3CF_2CH_2OC^{\bullet}H_2$ (P2) radicals can obtained from the reported $\Delta_rH°_{298}$ values for reactions 5.1.1 and 5.1.2 in Table 5.1.3, the calculated $\Delta_fH°_{298}$ value for $CF_3CF_2CH_2OCH_3$ and the experimental $\Delta_fH°_{298}$ values for H_2O (-57.8 kcal mol^{-1}) and OH (8.93 kcal mol^{-1}) radical. The $\Delta_fH°_{298}$ values for P1 and P2 are found to be -263.25 and -259.68 kcal mol^{-1}, respectively.

Table 5.1.3 The value of $\Delta_fH^0_{298}$ (in kcal mol^{-1}) for the reactant and product radicals calculated at M06-2X/6-31+G(d,p) from the isodesmic reactions with literature values

Species	**Reaction Schemes**	**Our Work $\Delta_fH^0_{298}$**	**Literat. Value[a] $\Delta_fH^0_{298}$**
$CF_3CF_2CH_2OCH_3$	R5	-307.20	-309.27
	R6	-307.99	
	R7	-308.49	
	Average	-307.89	
$CF_3CF_2C^{\bullet}HOCH_3$ (P1)		-263.25	
$CF_3CF_2CH_2OC^{\bullet}H_2$ (P2)		-259.68	

[a] Ref. [27]

5.1.3.2 Rate constant calculations

Canonical Transition State Theory (CTST) [29] has been used to obtained rate constant by using the equation given as:

$$k=\sigma\Gamma(T)\frac{k_BT}{h}\frac{Q_{TS}}{Q_A.Q_B}\exp\frac{-\Delta E^{\#}}{RT} \qquad (5.1.1)$$

Where, σ is the reaction path degeneracy, Γ(T) is the tunneling correction factor at temperature T. Q_{TS}, Q_A and Q_B are the total partition functions (per unit volume) for the transition states and reactants, respectively. $\Delta E^{\#}$ is the barrier height including zero point energy correction, k_B is the Boltzmann constant, h is the Planck's constant and R represents the universal gas constant. The tunneling correction was estimated by using the Eckart's unsymmetrical barrier method [30,31]. Except for the lowest vibrational mode, we have treated the entire vibrational modes quantum mechanically as separable harmonic oscillators. For the lowest-frequency mode, the partition function was calculated with the help of hindered-rotor approximation as proposed by Chuang and Truhlar [32].

We have also corrected electronic partition function of OH to obtained total partition function as the excited state of the OH radicals have a 140 cm^{-1} splitting due to spin-orbit coupling. The pre- and post-reactive complexes are considered on determination of reaction kinetics in this work as proposed Singleton and Cvetanovoic [33]. The computed rate constant values in the temperature range of 250-450 K are recorded in Table 5.1.4. At 298 K, our calculated k_{OH} value using M06-2X/6-31+G(d,p) barrier heights is 3.59×10^{-13} cm^3 $molecule^{-1}$ s^{-1} which is in a reasonable agreement with the experimental value of $(5.78 \pm 1.02) \times 10^{-13}$ cm^3 $molecule^{-1}$ s^{-1} reported by Thomsen *et al.*[23] and $(6.42 \pm 0.33)\times10^{-13}$ cm^3 $molecule^{-1}$ s^{-1} by Oyaro *et al.* [8]. However, our calculated rate constant (3.59×10^{-13} cm^3 $molecule^{-1}$ s^{-1}) is in very good agreement with the value of 3.93×10^{-13} cm^3 $molecule^{-1}$ s^{-1} estimated empirically by Urata *et al.* [10] using the artificial neural network (ANN) technique. Although, rate constants for H-abstraction from the $–CH_3$ group is found to be somewhat higher than that from the $–CH_2$ group for $CF_3CF_2CH_2OCH_3$ + OH reactions. Of course the H-abstraction from the $–CH_2$ group is thermodynamically more favourable due to its more exothermic nature.

Table 5.1.4 Rate constant values (in cm^3 $molecule^{-1}$ s^{-1}) for H-abstraction reactions of $CF_3CF_2CH_2OCH_3$ with OH radicals at M06-2X/6-31+G(d,p) level.

T (K)	k_{TS1}	k_{TS2a}	k_{TS2b}	k_{OH}
250	1.59×10^{-13}	2.95×10^{-14}	1.49×10^{-13}	3.37×10^{-13}
298	1.31×10^{-13}	2.85×10^{-14}	2.00×10^{-13}	3.59×10^{-13}
300	1.30×10^{-13}	3.91×10^{-14}	1.33×10^{-13}	3.01×10^{-13}
350	1.14×10^{-13}	5.08×10^{-14}	1.24×10^{-13}	2.89×10^{-13}
400	1.06×10^{-13}	6.48×10^{-14}	1.22×10^{-13}	2.92×10^{-13}
450	1.01×10^{-13}	8.08×10^{-14}	1.20×10^{-13}	3.02×10^{-13}

5.1.3.2 Atmospheric consequences

5.1.3.2.1 Atmospheric lifetime

Environmental processes such as photolysis, wet and dry deposition and reaction with atmospheric oxidants like OH radicals, Cl atoms, O_3 and NO_3 radicals are responsible for the atmospheric sink of VOCs. Previous studies [34,35] reported that photolysis and reactions with NO_3 and O_3 radicals are to be unimportant. The hydrophobic nature and volatility of ethers will render wet deposition and dry deposition an unlikely removal process. Thus, atmospheric lifetime (τ_{eff}) of HFEs is mainly occurring by OH-initiated H-abstraction. The lifetime estimations for HFEs are generally calculated at 272K on the basis of gas-phase removal by OH only and with methyl chloroform (MCF) [36] as reference:

$$\tau_{OH}^{HFE} = \frac{k_{MCF}\ (272\,K)}{k_{HFE}\ (272\,K)}\ \tau_{OH}^{MCF} \qquad (5.1.2)$$

Where, τ_{OH}^{HFE} is the lifetime for HFE-365mcf3, k_{HFE} and k_{MCF} are the rate constants for the reactions of OH radicals with HFE-365mcf3 and methyl chloroform (MCF), respectively at T = 272 K and τ_{OH}^{MCF} = 5.99 years [37]. Taking the values of rate constants for $k_{MCF} = 6.14\times10^{-15}$ from the report of Bravo *et al.* [37] and calculated rate constant of $k_{HFE} = 3.17\times10^{-13}$ cm^3 $molecule^{-1}$ s^{-1} at 272 K, the estimated lifetime is found to be 42 days which is in a reasonable agreement with the previous reported value of 20 days by Thomsen *et al.* [9].

5.1.3.3 Atmospheric fate of alkoxy radical

In order to explore the nature of the reaction mechanism for the unimolecular decomposition of $CF_3CF_2CH(O^{\bullet})OCH_3$ and $CF_3CF_2CH_2OCH_2O^{\bullet}$ radicals in the gas phase, theoretical calculations at the M06-2X/6-31+G(d,p) level of theory are carried out. The reactions are envisaged to occur via reactions (5.1.3-5.1.7). Figure 5.1.1 shows the optimized geometries of radicals and transition states involved in these reactions obtained at the M06-2X/6-31+G(d,p) level. Transition states obtained on the potential energy surfaces of reactions (R3-R7) are characterized as TS3, TS4, TS5, TS6 and TS7, respectively. The search was made along the minimum energy path on a relaxed potential energy surface. The calculated harmonic vibrational frequencies of the stationary points are given in Table B.2 of Appendix B. These results show that the reactant and products have only real and positive vibrational frequencies and thus they have stable minima on their potential energy surface. On the other hand, all the transition states TS3, TS4, TS5, TS6 and TS7 are characterized by one imaginary frequencies obtained at 450i, 1029i, 1284i, 1047i and 1539i cm^{-1}, respectively. The existence of these transition states on the potential energy surface are further supported by intrinsic IRC calculation performed at the same level of theory. The thermochemical data calculated at M06-2X/6-31+G(d,p) level are summarized in Table 5.1.6. Free energy values show that two reaction channels (5.1.5 and 5.1.7) are significantly exergonic ($\Delta G < 0$) and thus thermodynamically more facile. Results also reveal that reaction channels 5.1.4 and 5.1.6 proceeds with endothermicity of 6.79 and 6.59 kcal mol^{-1},respectively. This predicts that reactions 5.1.4 and 5.1.6 are unimportant in comparison to reactions 5.1.3, 5.1.5 and 5.1.7 as listed in Table 5.1.5.

Table 5.1.5 Values of $\Delta_rH°_{298}$ and $\Delta_rG°_{298}$ (in kcal mol^{-1}) for reactions (R3-R7) involved in thermal decomposition of radicals at M06-2X level of theory.

Reaction Channels	**$\Delta_rH°_{298}$**	**$\Delta_rG°_{298}$**
Reaction Channel 5.1.3	-3.39	-16.77
Reaction Channel 5.1.4	6.79	-1.52
Reaction Channel 5.1.5	-41.29	-43.13
Reaction Channel 5.1.6	6.59	-0.63
Reaction Channel 5.1.7	-41.49	-42.24

The energy barriers corresponding to reactions (5.1.3-5.1.7) calculated at M06-2X/6-31+G(d,p) level of theory are provided in Table 5.1.6. The energy barrier for H-abstraction reaction of $CF_3CF_2CH(O^{\bullet})OCH_3$ radical with molecular O_2 is found to be 4.48 kcal mol^{-1} whereas the same for C-C bond scission is found to be 5.89 kcal mol^{-1} at M06-2X/6-31+G(d,p) level of theory. The calculated energy barriers for reactions (5.1.3-5.1.5) clearly show that the oxidative pathways (5.1.5) is the dominant reaction pathway and C-C bond scission reaction (5.1.3) is less important for atmospheric degradation of $CF_3CF_2CH(O^{\bullet})OCH_3$ radical which is in accord with the conclusion made by Oyaro *et al.* [8] but contradict with the experimental finding of Thomsen *et al.* [9]. Similarly, the energy barriers for H-abstraction reaction of $CF_3CF_2CH_2OCH_2O^{\bullet}$ radical for C-H bond scissions and hydrogen abstraction by O_2 are estimated to be 14.41 and 9.84 kcal mol^{-1}, respectively. It is obvious from Table 5.1.7 that the barrier height (9.84 kcal mol^{-1}) for oxidation of $CF_3CF_2CH_2OCH_2O^{\bullet}$ radical with O_2 is considerably lower than that for C-H bond scission and the dominant oxidative pathways of this alkoxy radical in the atmosphere is thus visualized. We, therefore, can say that the atmospheric fate of $CF_3CF_2CH_2OCH_2O^{\bullet}$ radical is reaction with O_2 leading to the formation of $CF_3CF_2CH_2OCHO$ which is in accordance with the experimental findings of Thomsen *et al.* [9].

Table 5.1.6 Calculated barrier heights (in kcal mol^{-1}) for reactions (R3-R7) at M06-2X level of theory

Reaction Channels	**M06-2X/ 6-31+G(d,p)**
$CF_3CF_2CH(O^{\bullet})OCH_3$	
TS3 (C-C bond scission)	5.89
TS4 (C-H bond scission)	14.21
TS5 (Reaction with O_2)	4.48
$CF_3CF_2CH_2OCH_2O^{\bullet}$	
TS6 (C-H bond scission)	14.41
TS7 (Reaction with O_2)	9.84

5.1.4 SALINT OBSERVATIONS

We have investigated here the potential energy surface and reaction kinetics of the H atom abstraction reaction of $CF_3CF_2CH_2OCH_3$ with OH radicals at M06-2X/6-31+G(d,p) level of theory. The main outcomes of this study are as follows:

1. The reaction with OH radicals is followed an indirect path i.e. reaction proceeds via the pre- and post- reaction complexes.
2. The barrier height for hydrogen abstraction by OH radicals from $-CH_2$ and $-CH_3$ groups are found to be -0.21, 2.68 and 0.14 kcal mol^{-1}, respectively.
3. The thermal rate constant for the $CF_3CF_2CH_2OCH_3$ + OH reaction is found to be 3.59×10^{-13} cm^3 $molecule^{-1}$ s^{-1} using canonical transition state theory at 298 K and it agrees with experimental finding.
4. H-abstraction from $-CH_2$ group is more exothermic than that from $-CH_3$ group. The $\Delta_f H°_{298}$ for $CF_3CF_2CH_2OCH_3$, $CF_3CF_2C^{\bullet}HOCH_3$ and

$CF_3CF_2CH_2OC^{\bullet}H_2$ species calculated from M06-2X results are -307.89, -263.25 and -259.68 kcal mol^{-1}, respectively. The D^0_{298} value obtained for the C–H bonds in the $–CH_2$ and $–CH_3$ sites of $CF_3CF_2CH_2OCH_3$ amount to 96.78 and 100.35 kcal mol^{-1} respectively.

5. The OH-driven atmospheric lifetime of $CF_3CF_2CH_2OCH_3$ is estimated to be 42 days.
6. The results show that the reaction with O_2 is the sole atmospheric fate for decomposition of $CF_3CF_2CH_2OCH_2O^{\bullet}$ radical.

5.2 ATMOSPHERIC CHEMISTRY OF HFE-7000 (i-$C_3F_7OCH_3$) AND ISOFLUORO-PROPYL FORMATE (i-$C_3F_7OC(O)H$)

5.2.1 INTRODUCTION

Segregated hydrofluoroethers are VOCs in which fluorocarbons and hydrocarbons are present in two terminals of the oxygen atom. They are now used in various applications such as industries and laboratories. To know the full insight of the atmospheric chemistry of these compounds is necessary from environmental point of view. The OH and Cl-initiated oxidation of HFE-7000 are experimentally reported by many groups [38-41].The present work focuses on quantum calculations on the H-abstraction reactions between i-HFE-7000 and OH radicals using DFT methods. Our calculations implies that only two reaction channels are feasible for i-$C_3F_7OCH_3$ + OH reactions as shown below:

(5.2.1a and 5.2.1b)

The reaction of i-HFE-7000 with OH radicals was studied by Tokuhashi *et al.*[38] over the temperature range of 250-430 K and reported the Arrhenius expression: k(T) = $1.98^{+0.48}_{-0.38} \times 10^{-12} \exp[-(1450 \pm 70)/T]$ cm^3 $molecule^{-1}$ s^{-1} with room temperature rate coefficient value of (1.52 ± 0.06) $\times 10^{-14}$ cm^3 $molecule^{-1}$ s^{-1}. In a recent study, Andersen *et al.*[42] investigated the kinetics of the reactions of i-$C_3F_7OCH_3$ using FTIR Smog Chamber technique and reported rate constant values as k(OH + i-$C_3F_7OCH_3$) = (1.55±0.24) $\times 10^{-14}$ and k(Cl + i-$C_3F_7OCH_3$) = (1.80 ± 0.42) $\times 10^{-13}$ cm^3 $molecule^{-1}$ s^{-1} at 298 K, respectively. However, for reaction 5.2.1, Urata *et al.* [10] empirically estimated a value of 0.59 × 10^{-14} cm^3 $molecule^{-1}$ s^{-1} on the basis of bond dissociation enthalpies (BDE's) of the C–H bond using the artificial neural network (ANN) technique.

The experimental or theoretical study to elucidate the dissociative pathways of i-$C_3F_7OCH_2O^•$ radical derived from one of the important classes of hydrofluoroethers (i-HFE-7000) is still missing. There are three potential pathways of decomposition of i-

$C_3F_7OCH_2O^\bullet$ radical that involve bond scissions and oxidation processes. These are represented as follows:

$$i\text{-}C_3F_7OCH_2O^\bullet \longrightarrow i\text{-}C_3F_7O^\bullet + CH_2O \quad (5.2.2)$$

$$\longrightarrow i\text{-}C_3F_7OC(O)H + H \quad (5.2.3)$$

$$+ O_2 \longrightarrow i\text{-}C_3F_7OC(O)H + HO^\bullet_2 \quad (5.2.4)$$

The thermochemical studies have been performed to analyze the stability of all the species involved in the reactions. In present study we have also study the OH and Cl-atom initiated hydrogen abstraction reaction from the FES generated from the HFE i.e.; isofluoro-propyl formate ($i\text{-}C_3F_7OC(O)H$). Our calculations suggest that two reaction channels are feasible for $i\text{-}C_3F_7OC(O)H$ + OH/Cl reactions as given below.

$$i\text{-}C_3F_7OC(O)H + OH \longrightarrow i\text{-}C_3F_7OC(O) + H_2O \quad (5.2.5)$$

$$i\text{-}C_3F_7OC(O)H + Cl \longrightarrow i\text{-}C_3F_7OC(O) + HCl \quad (5.2.6)$$

Literature survey reveals that no experimental or theoretical study on OH-initiated hydrogen abstraction of $i\text{-}C_3F_7OC(O)H$ is reported so far. However, Chen *et al.*[43] studied the kinetics of the reaction of OH radical with $n\text{-}C_3F_7OC(O)H$ using FTIR technique over the temperature range of 253-328 K and reported rate constant at 298 K as $(2.04 \pm 0.04)\times10^{-14}$ cm^3 $molecule^{-1}$ s^{-1}. Andersen *et al.* [42] reported the kinetics for reaction R6 with a rate constant value as $k(Cl + i\text{-}C_3F_7OC(O)H) = (1.47 \pm 0.56)\times10^{-14}$ cm^3 $molecule^{-1}$ s^{-1} at 298 K. This is the first detailed theoretical study of H-abstraction reactions of i-HFE-7000 with atmospheric oxidants (OH radicals). We also present BDE of the C-H bond in $i\text{-}C_3F_7OCH_3$. In addition, enthalpy of formation ($\Delta_fH°_{298}$) for $i\text{-}C_3F_7OCH_3$ and radical ($i\text{-}C_3F_7OC^\bullet H_2$) are computed using isodesmic work reactions at M06-2X/6-31+G(d,p) level.

5.2.2 COMPUTATIONAL DETAILS

The computational methodologies are similar as that of the previous section. Geometry optimization of the species are made at the M06-2X [14] level of theory using 6-31+G(d,p) basis set. Since the formation of pre- and post-reaction complex

modifies the shape of potential energy surface for the hydrogen abstraction reactions and hence affects the tunneling factor. As a result the rate constant for hydrogen abstraction also changes. Therefore, we also validated pre- and post reactive complexes along the entry and exit of the reaction path. In order to determine the nature of different stationary points on the potential energy surface, vibrational frequencies calculations were performed using the same level of theory at which the optimization was made. The intrinsic reaction coordinates (IRC) calculations [23] for the forward and reverse directions beginning from each TS point are also performed at the M06-2X/6-31+G(d,p) level to ascertain the correct connections. Single point energy calculations were performed at M06-2X in conjunction with 6-311++G(d,p) basis set. The 6-311++G(d,p) is a valence triple-ζ quality basis set with single polarization and double diffuse functions on all atoms. All the calculations are performed with the Gaussian 09 suite of program [13].

5.2.3 RESULTS AND DISCUSSIONS

5.2.3.1 Structure and energetics

The thermochemical data for the reaction of i-$C_3F_7OCH_3$ with OH radicals at both levels are recorded in Table 5.2.1. Thermal corrections to the energy at 298 K are also included in the determination of these thermodynamic functions. The enthalpy of reaction values indicates that the reaction 5.2.1 is significantly exothermic in nature. It can be seen from the geometrical parameters and stereographical orientation, the hydrogen atoms in the $–CH_3$ group are not equivalent. The stereographic environment of one H-atom (C1-H3) is different from the other two (C1-H1 and C1-H2) in the $–CH_3$ group as depicted in Figure 5.2.1. Thus two transition states should be located for i-$C_3F_7OCH_3$ + OH reactions. Therefore, we have located two transition states (TS1a and TS1b) for reactions 5.2.1a and 5.2.1b, respectively.

Table 5.2.1 Thermochemical data for reaction channels (R1-R6) and bond dissociation enthalpy (D^0_{298}) calculated at M06-2X/6-31+G(d,p) and M06-2X/6-311++G(d,p) (within parentheses) levels of theory along with literature value. All values are in kcal mol^{-1}.

Reaction Channels	**$\Delta_r H°_{298}$**	**$\Delta_r G°_{298}$**
Reaction 5.2.1	-16.23 (-16.60)	-17.43 (-17.80)
Reaction 5.2.2	21.85 (21.03)	9.40 (8.59)
Reaction 5.2.3	15.33 (14.19)	7.38 (6.24)
Reaction 5.2.4	-32.75 (-32.95)	-34.22 (-34.42)
Reaction 5.2.5	-18.68 (-19.07)	-19.70 (-20.10)
Reaction 5.2.6	-2.35 (-3.55)	-4.60 (5.81)
D^0_{298}		**Literature value**
i-$C_3F_7OC^*H_3$	101.63 (101.19)	101.94[a]

[a] Ref. [10]

In the entrance channel for reaction R1, pre- reactive complexes (RC1a and RC1b) have been located from IRC calculations in the present work. In the exit channel, there are also product complexes occurring before the release of the final products, which are labeled as PC1a and PC1b. In pre-reactive complex RC1a, three hydrogen bonds are formed between the O2…H3, O1…H4 and F4…H4 bonds with the bond distances of 2.582, 2.414 and 2.246 Å, respectively. However, in the complex RC1b, the two hydrogen bonds are formed between the O2…H2, and F2…H4 bonds with the bond distances of 2.358 and 2.472 Å, respectively while the other bond lengths are very close to those in equilibrium structures of i-$C_3F_7OCH_3$ molecule. Simultaneously, the post-reaction complexes (PC1a and PC1b) with energy less than the corresponding products are located at the exits of the reaction channels which can be identified with relatively strong C–H…O and O-H…F bonds, as provided in Figure 5.2.2. Thus it is clear that the reaction channels (R1a and R1b) may proceed via indirect mechanisms.

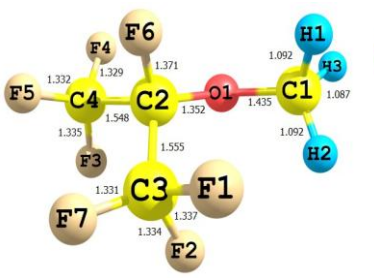

i- $C_3F_7OCH_3$

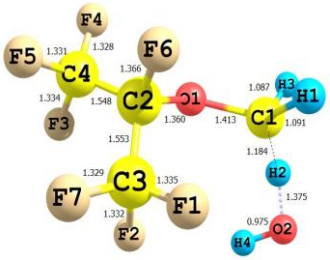

TS1a

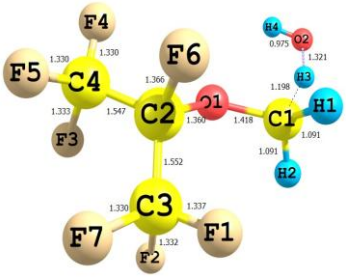

TS1b

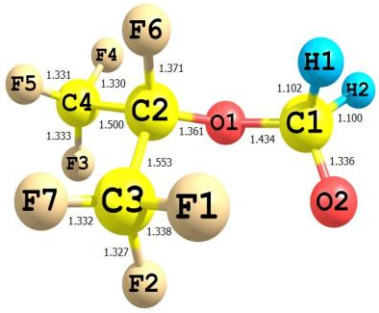

i- $C_3F_7OCH_2O^{\bullet}$

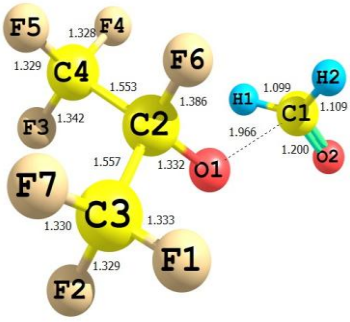

TS2

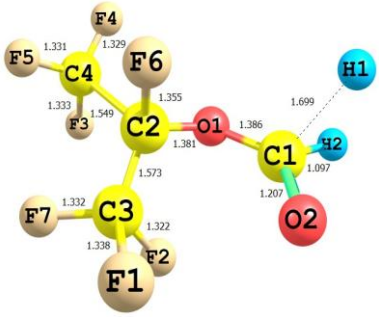

TS3

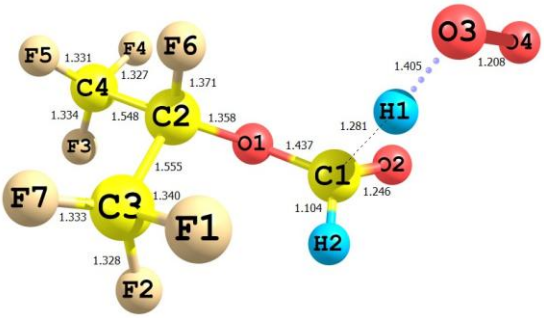

TS4

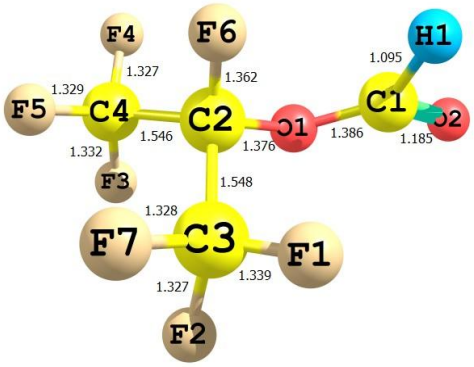

i- $C_3F_7OC(O)H$

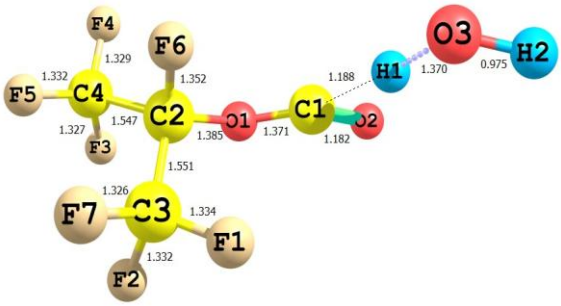

TS5

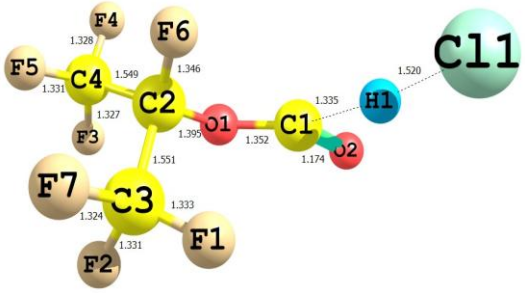

TS6

Figure 5.2.1 Optimized geometries of reactants and transition states at M06-2X/6-31+G(d,p) level of theory. Bond lengths are in Angstroms.

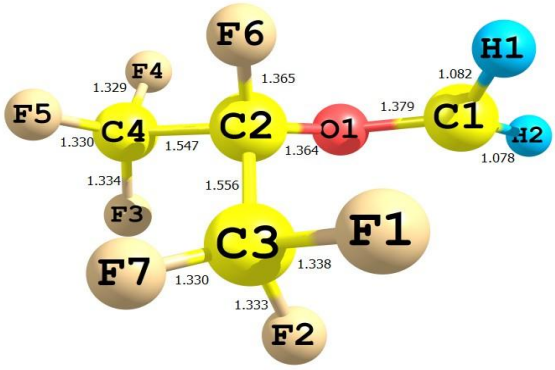

i- $C_3F_7OC^{\bullet}H_2$

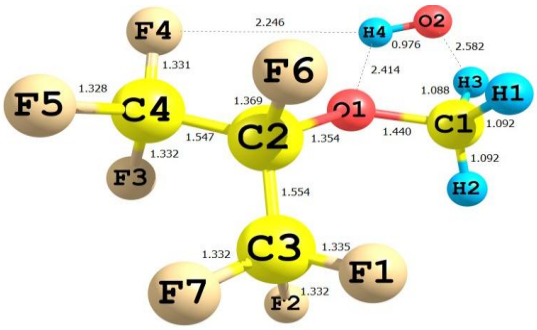

RC1a

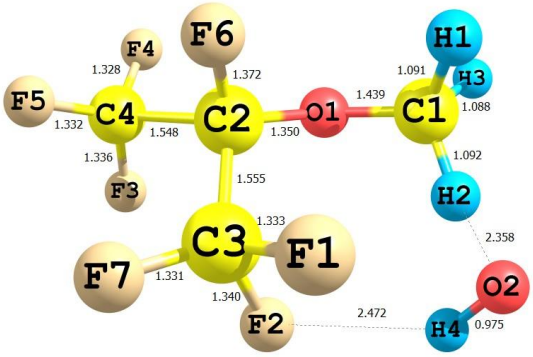

RC1b

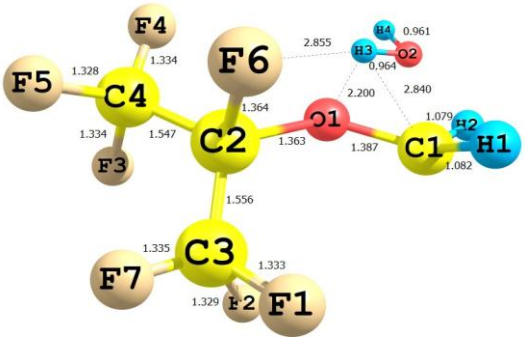

PC1a

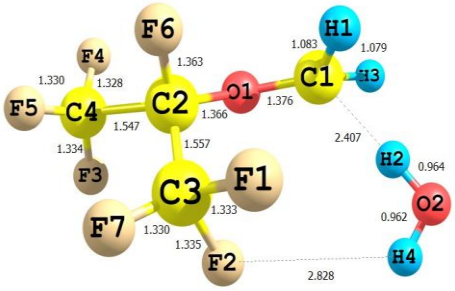

PC1b

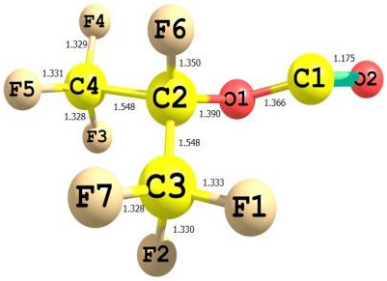

i- $C_3F_7OC(O)$

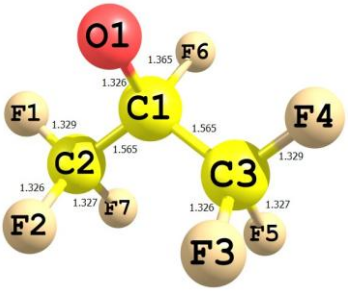

i- $C_3F_7O^{\bullet}$

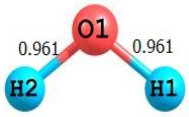

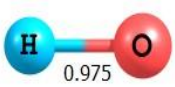

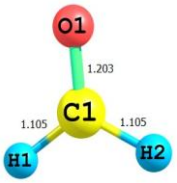

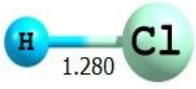

Figure 5.2.2 Optimized geometries of reactant complexes, product complexes and products at M06-2X/6-31+G(d,p) level of theory. Bond lengths are in Angstroms.

Optimized geometries of reactants and transition states are shown in Figure 5.2.1, whereas the same for reactant complexes, product complexes and products obtained at the M06-2X/6-31+G(d,p) level are shown in Figure 5.2.2. During the formation of transition states, the important structural parameters have to be observed are one of the C-H bond of the leaving hydrogen and the newly formed bond between H and O atoms in the OH radicals. In the optimized structures of TS1a and TS1b for reaction 5.2.1, the length of the breaking C-H bonds are found to be longer in range of 8.42-10.21% than the than the observed C-H bond length in isolated i-$C_3F_7OCH_3$ molecule whereas the forming O...H bond length is longer by 37.46-43% than the O-H bond length in H_2O. The fact that the elongation of forming bond is larger than that of the breaking bond indicates that the barrier of the reaction (5.2.1) is near the corresponding reactants. This means the reaction will proceeds via early transition state structure which is in consonance with Hammond's postulate [24] applied to an exothermic hydrogen abstraction reaction.

The results obtained from frequency outputs for all species are provided in Table B3 of Appendix B. These results show that all the stable species minima on their potential energy surface and these are confirmed by the occurrence of only real vibrational frequencies. Transition vectors for all the transition states are obtained at 1136i and 1381i cm^{-1} for TS1a and TS1b, respectively. Intrinsic reaction coordinate (IRC) calculations for the TSs are also performed at the same level of theory which smoothly connects transition states via reactant to product side. The relative energies (including ZPE) for all the species involved in reaction channels (5.2.1a and 5.2.1b) obtained at M06-2X/6-31+G(d,p) level are given in Table 5.2.2. From the table, we can see that energy barriers for the i-$C_3F_7OCH_3$ + OH reaction for 5.2.1a and 5.2.1b are 2.43 and 3.80 kcal mol^{-1}, respectively at M06-2X/6-311++G(d,p) level of theory; whereas the same from M06-2X/6-31+G(d,p) results are found to be 2.13 and 3.46 kcal mol^{-1}, respectively. The potential energy diagram of the title reaction is shown in Figure 5.2.3. For the generation of energy profile diagram, zero-point energy corrected total energy data as recorded in Table 5.2.2 are taken. These energies are plotted with respect to the ground state energy of i-$C_3F_7OCH_3$ + OH including ZPE arbitrarily taken as zero. Furthermore, spin contamination is not an issue for the i-$C_3F_7OCH_3$ + OH

reactions because $<S^2>$ is found to be 0.76 before annihilation that is only slightly larger than the expected value of $<S^2> = 0.75$ for doublets at M06-2X level.

Table 5.2.2 Relative energies ΔE, (in kcal mol^{-1}) with zero-point energy correction for the reactants, reaction complexes, transition states, product complexes and products at M06-2X levels of theory.

Species	**M06-2X/ 6-311++G(d,p)**	**M06-2X/6-31+G(d,p)**
i-$C_3F_7OCH_3$ + OH/Cl	0.00	0.00
RC1a	-4.08	-3.91
RC1b	-2.43	-2.26
TS1a	2.43	2.13
TS1b	3.80	3.46
PC1a	-20.23	-19.86
PC1b	-20.15	-18.41
i-$C_3F_7OC^{\bullet}H_2$ + H_2O	-16.89	-16.52

The standard enthalpy of formation ($\Delta_fH°_{298}$) for i-$C_3F_7OCH_3$ and i-$C_3F_7OC^{\bullet}H_2$ is valuable information for understanding the mechanism and thermochemical properties of their reactions. The group-balanced isodesmic reactions are applied to obtain the value of $\Delta_fH°_{298}$ as shown below in reaction (5.2.7-5.2.12).

$(CF_3)_2CFOCH_3 + CH_4 + CH_3F \longrightarrow CF_3CH_2CF_3 + CH_3OCH_3 + CH_2F_2$ (5.2.7)

$(CF_3)_2CFOCH_3 + CH_4 \longrightarrow (CF_3)_2CHOCH_3 + CH_3F$ (5.2.8)

$(CF_3)_2CFOCH_3 + CH_4 \longrightarrow CF_3CF_2CH_2OCH_3 + CH_2F_2$ (5.2.9)

$(CF_3)_2CFOCH_2 + CH_4 \longrightarrow (CF_3)_2CFOCH_3 + CH_3$ (5.2.10)

$(CF_3)_2CFOCH_2 + CH_4 + CH_3F \longrightarrow CHF_2CF_2CH_2F + CH_3OCH_3 + CF_3$ (5.2.11)

$(CF_3)_2CFOCH_2 + CH_4 \longrightarrow CF_3CF_2CH_2OCH_3 + CHF_2$ (5.2.12)

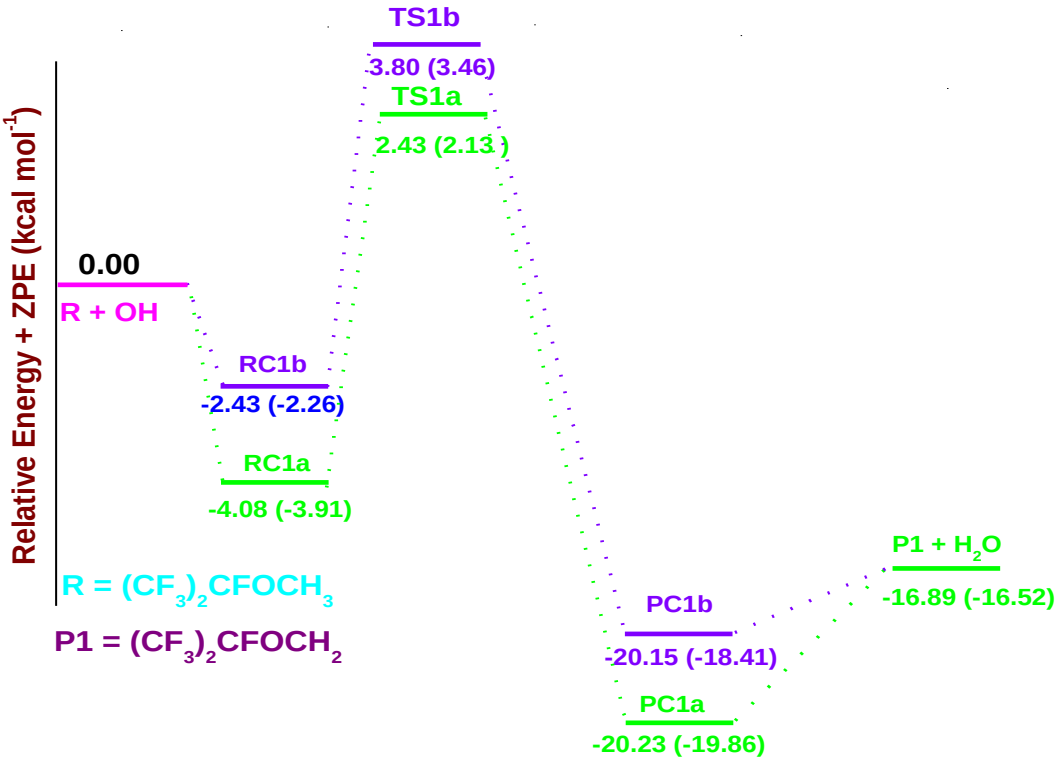

Figure 5.2.3 Potential energy diagram for i-$C_3F_7OCH_3$ + OH reactions at M06-2X/6-311++G(d,p) level. The calculated values at M06-2X/6-31+G(d,p) level of theory are provided in parentheses.

All the species involved in the isodesmic reactions (5.2.7-5.2.12) are optimized and reaction enthalpies ($\Delta_rH°_{298}$) are calculated at the M06-2X/6-31+G(d,p) level of theory. The experimental $\Delta_fH°_{298}$ values for CH_4: -17.9 kcal mol^{-1}, CF_2CF_2: -157.40 kcal mol^{-1}, $CF_3CF_2CH_2OCH_3$: -309.99 kcal mol^{-1}, CH_2FCF_3: -214.10 kcal mol^{-1}, $CF_3CHFOCH_3$: -257.23 kcal mol^{-1} and CF_3CF_3: -320.88 kcal mol^{-1} are taken from previous report of Kondo *et al.* [28] and that for CHF_2: -58.07 kcal mol^{-1}, CHF_3: -166.08 kcal mol^{-1}, CH_3: 34.82 kcal mol^{-1} and CF_3: -111.75 kcal mol^{-1} are taken from the data of Csontos *et al.* [27] to obtain the required enthalpies of formation. The

calculated values of enthalpies of formation at both levels are listed in Table 5.2.3. We can see from the table that the values of $\Delta_fH°_{298}$ for the species obtained by the three working chemical reactions at both levels are consistent with each other. The average $\Delta_fH°_{298}$ for i-$C_3F_7OCH_3$ and i-$C_3F_7OC^{\bullet}H_2$ radical calculated from M06-2X/6-31+G(d,p) results are -414.67 and -365.19 kcal mol^{-1}, respectively; whereas the same from M06-2X/6-311++G(d,p) results are found to be -413.83 and -364.78 kcal mol^{-1}, respectively. The calculated value of $\Delta_fH°_{298}$ at M06-2X/6-31+G(d,p) level for i-$C_3F_7OCH_3$ is found in good agreement with the theoretical value of -414.43 kcal mol^{-1} by Kondo *et al.* [28].

Table 5.2.3 The values $\Delta_fH°_{298}$ (in kcal mol^{-1}) for the species from the isodesmic reactions are given at M06-2X/6-31+G(d,p) and M06-2X/6-311++G(d,p) levels

Species	**Reaction Schemes**	**M06-2X/6-31+G(d,p)**	**M06-2X/6-311++G(d,p)**	**Literature Value[a]**
i-$C_3F_7OCH_3$	5.2.7	-412.31	-411.80	-414.43
	5.2.8	-416.63	-415.74	
	5.2.9	-415.09	-413.97	
Average		-414.67	-413.83	
i-$C_3F_7OC^{\bullet}H_2$	5.2.10	-366.43	-366.06	
	5.2.11	-362.59	-361.80	
	5.2.12	-366.57	-366.50	
Average		-365.19	-364.78	

[a] Ref. [28]

The obtained bond-dissociation energy, BDE ($D°_{298}$) of the C-H bond of i-$C_3F_7OCH_3$ molecule along with literature value is given in Table 5.2.1. The $D°_{298}$ value revealed from the M06-2X/6-31+G(d,p) and M06-2X/6-311++G(d,p) result for C–H bond of i-$C_3F_7OCH_3$ amount to be 101.63 and 101.19 kcal mol^{-1}, respectively. We can observe that the calculated BDE values for the C–H bond is in very close agreement with the reported theoretical value of 101.94 kcal mol^{-1} reported by Urata *et al.*[10] using ANN technique .

5.2.3.2 Rate constant calculation

The rate constant for title reactions are evaluated using conventional transition state theory (TST) [29] equation:

$$k=\sigma\Gamma(T)\frac{k_B T}{h}\frac{Q_{TS}}{Q_A . Q_B}\exp\frac{-\Delta E^{\#}}{RT} \quad (5.2.1)$$

Where, σ is the reaction path degeneracy accounting for the number of equivalent H-atoms, $\Gamma(T)$ is the tunneling correction factor at temperature T. The σ value for R1 is taken as 2 because three H-atoms present in the $-CH_3$ group are not equivalent. Q_{TS}, Q_A and Q_B are the total partition functions (per unit volume) for the transition states and reactants, respectively. $\Delta E^{\#}$ is the barrier height including zero point energy correction, k_B is the Boltzmann constant, h is the Planck's constant and R represents the universal gas constant. The tunneling correction was estimated by using the Eckart's unsymmetrical barrier method [29,44].

The partition functions for reactants and transition states are evaluated by the harmonic oscillators approximation. In the calculation of reactant electronic partition function, the excited state of the OH radicals is included, with a 140 cm^{-1} splitting due to spin-orbit coupling. The procedure proposed by Singleton and Cvetanovic [32] are incorporated for taking into consideration the effect of pre- and post-reactive complex on reaction kinetics. The computed rate constant values in the temperature range of 250-450 K are recorded in Table 5.2.4. It can be seen that our calculated k_{OH} value (2.36×10^{-14} cm^3 $molecule^{-1}s^{-1}$) using M06-2X/6-311++G(d,p) results at 298 K, is in a reasonable agreement with the experimental values of $(1.52 \pm 0.06) \times 10^{-14}$ and $(1.55 \pm 0.24)\times10^{-14}$ cm^3 $molecule^{-1}s^{-1}$ reported by Tokuhashi *et al.*[38] and Andersen *et al.*[42] respectively. However, the rate coefficient obtained from the M06-2X/6-31+G(d,p) results (3.76×10^{-14} cm^3 $molecule^{-1}$ s^{-1}) overestimates the experimental values at 298 K. This may be due to the fact that experimentally only one reaction channel is assumed for i-$C_3F_7OCH_3$ + OH reactions; whereas theoretically, two transition states are feasible for the titled reaction due to presence of two different H-atoms in $-CH_3$ group.

Temperature variation of k_{OH} result obtained at M06-2X levels along with the experimental results is shown in Figure 5.2.4. Finally, the overall rate constants within the temperature range 250–450 K are fitted by using Arrhenius equation as follows: $k = 3.96\times 10^{-13} \exp[(-842.03 \pm 45.50)/T]$ cm^3 $molecule^{-1}$ s^{-1}.

Table 5.2.4 Rate coefficient values (in cm^3 $molecule^{-1}$ s^{-1}) for reactions R1a and R1b and total rate coefficient (k_{OH}) values as calculated at M06-2X level of theories.

Methods	**M06-2X/6-31+G(d,p)**			**M06-2X/6-311++G(d,p)**		
Temp (K)	$\mathbf{k_{TS1a}}$	$\mathbf{k_{TS1b}}$	$\mathbf{k_{OH}}$	$\mathbf{k_{TS1a}}$	$\mathbf{k_{TS1b}}$	$\mathbf{k_{OH}}$
250	1.86×10^{-14}	8.97×10^{-15}	2.75×10^{-14}	1.11×10^{-14}	5.07×10^{-15}	1.61×10^{-14}
298	2.37×10^{-14}	1.39×10^{-14}	3.76×10^{-14}	1.52×10^{-14}	8.41×10^{-15}	2.36×10^{-14}
300	2.40×10^{-14}	1.41×10^{-14}	3.82×10^{-14}	1.53×10^{-14}	8.58×10^{-15}	2.38×10^{-14}
350	3.02×10^{-14}	2.14×10^{-14}	5.16×10^{-14}	2.05×10^{-14}	1.37×10^{-14}	3.42×10^{-14}
400	3.73×10^{-14}	3.07×10^{-14}	6.80×10^{-14}	2.63×10^{-14}	2.06×10^{-14}	4.69×10^{-14}
450	4.53×10^{-14}	4.23×10^{-14}	8.76×10^{-14}	3.32×10^{-14}	2.95×10^{-14}	6.27×10^{-14}

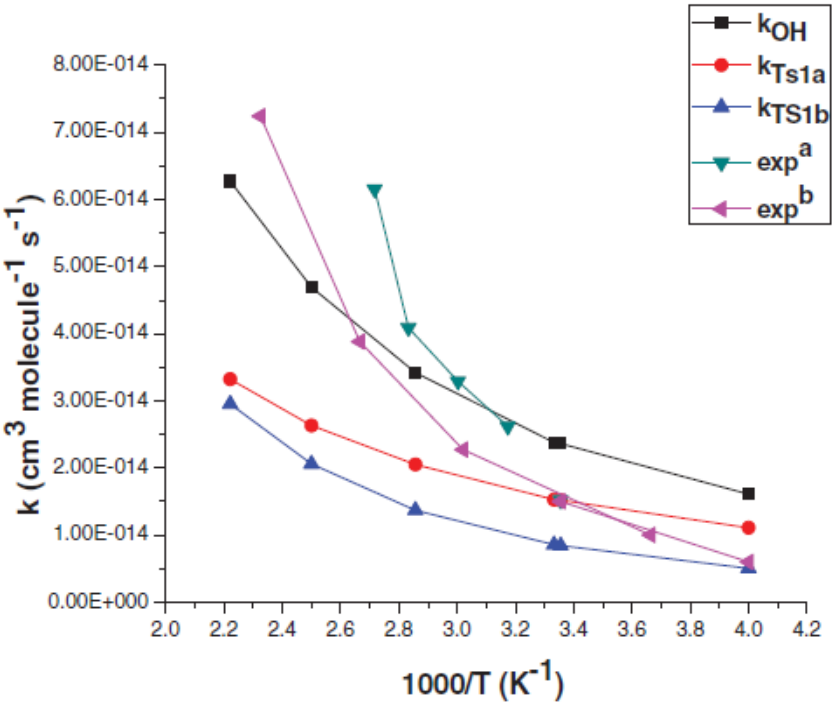

Figure 5.2.4 Rate constants for hydrogen abstraction reactions of i-$C_3F_7OCH_3$ with OH radicals and total rate constant (k_{OH}) for i-$C_3F_7OCH_3$ + OH reactions. [a]Ref. [38], [b]Ref. [40].

5.2.3 Atmospheric fate of alkoxy radical

The fate of alkoxy radical i-$C_3F_7OCH_2O^{\bullet}$ produced from the thermal decomposition in the atmosphere is predicted to occur via reactions (R2-R4). The thermodynamic calculations performed at M06-2X levels for reaction enthalpies ($\Delta_rH°_{298}$) and free energies ($\Delta_rG°_{298}$), associated with reaction channels (5.2.2-5.2.4) are recorded in Table 5.2.1. Results show that reaction channel (5.2.4) proceeds with high exothermicity of 32.75 kcal mol^{-1} along with a negative free energy change of 34.22 kcal mol^{-1}. This suggests that reaction channel (5.2.4) is thermodynamically the most favorable decomposition channel in comparison to reaction channels 5.2.2 and 5.2.3. Figure 5.2.1 shows the optimized geometries of reactant and transition states obtained at the M06-2X/6-31+G(d,p) level. Transition states resulted on the potential energy surfaces of reactions (5.2.2-5.2.4) are represented as TS2, TS3 and TS4,

respectively. In the optimized structure of TS2 the C-O bond (C1-O1) elongates from 1.434 to 1.966 Å (about 37%) with a simultaneous shrinkage (almost 11%) of the C1-O2 bond. Similarly, in TS3 of C1-H1 bond length elongates from 1.102 to 1.699 Å resulting in an increase of about 54% and at the same time shrinkage of the C1-O2 bond. The transition state TS4 for oxidative pathways reveals that C-H bond (C1-H1) increases from 1.102 to 1.281 Å (16%) leading to the formation of isofluoro-propyl formate (i-$C_3F_7OC(O)H$) and $HO^{\bullet}_2$ radical. Harmonic vibrational frequencies for reactant, products and transition states involved in reactions (5.2.2-5.2.4) are recorded in Table B.3 of Appendix B. These result shows that the transition states are characterized by the occurrence of only one imaginary frequency obtained at 540i, 1019i and 1724i cm^{-1} for TS2, TS3 and TS4, respectively.

Table 5.2.5 Calculated barrier heights for transition states involved in thermal decomposition of i-$C_3F_7OCH_2O^{\bullet}$ radical at various levels of theory. All values are in kcal mol^{-1}.

Reaction Channels	**M06-2X/6-31+G(d,p)**	**M06-2X/6-311++G(d,p)**
TS2 (C-O bond scission)	27.34	25.89
TS3 (C-H bond scission)	21.26	20.90
TS4 (Reaction with O_2)	10.31	18.73

The zero-point energy corrected energy barriers corresponding to reactions (5.2.2-5.2.4) at both levels are recorded in Table 5.2.5. Results show that the M06-2X/6-31+G(d,p) method yields a value of 35.41, 22.18 and 9.37 kcal mol^{-1} for TS2, TS3 and TS4, respectively. However, we are not able to avail experimental or theoretical data in the literature to compare the energy barriers associated with the decomposition channels of i-$C_3F_7OCH_2O^{\bullet}$ considered in the present investigation. The energy barrier for reaction with O_2 is reasonably lower than that for other decomposition pathways and the supremacy of the oxidative pathways of this alkoxy radical in the atmosphere is thus visualized. Hence, we emphasized here that the

atmospheric fate of i-$C_3F_7OCH_2O^{\bullet}$ radical is reaction with O_2 leading to the formation i- $C_3F_7OC(O)H$. This is in accord with the experimental findings of Wallington *et al.* [45] and Ninomiya *et al.*[46] for similar species ($C_4F_9OCH_2O^{\bullet}$ and n-$C_3F_7OCH_2O^{\bullet}$) where oxidation pathways dominant the fate of these radicals.

5.2.4 Atmospheric implications

5.2.4.1 Atmospheric lifetime

In order to minimize the errors resulting from neglecting the specific temperature dependences, when calculating OH-based lifetimes, the use of 272 K as an average tropospheric temperature and methyl chloroform (CH_3CCl_3), as a chemical of well known source and sink, has been suggested [47]. Thus, lifetime estimations for HFEs are generally calculated on the basis of gas-phase removal by OH only and with methyl chloroform (MCF) as reference:

$$\tau_{OH}^{HFE} = \frac{k_{MCF}\ (272\ K)}{k_{HFE}\ \ (272\ K)}\ \tau_{OH}^{MCF} \qquad (5.2.2)$$

Where τ_{OH}^{HFE} is the lifetime for HFE-7100, k_{HFE} and k_{MCF} are the rate constants for the reactions of OH radicals with HFE-7100 and methyl chloroform (MCF), respectively at T = 272 K and τ_{OH}^{MCF} = 5.7 years [47]. Taking the values of rate constants for k_{MCF} = 1.0×10^{-14} from [47] and calculated rate constant of k_{HFE} = 1.79×10^{-14} cm^3 $molecule^{-1}$ s^{-1} at 272 K, the estimated lifetime is found to be 3.19 years which is in a good agreement with the reported value of 3.7 years by Andersen *et al.* [42] and Hodnebrog *et al.*[48].

5.2.4.2 Fate of fluorinated ester

Figure 5.2.1 shows the optimized geometries of two transition states (TS5 and TS6). The thermochemical data involved in reactions (5.2.5-5.2.6) are given in Table 5.2.1. The results from the table reveal that reaction 5.2.5 is significantly exothermic in nature. Vibrational frequencies of the species are given in Table B.3 of Appendix B. Transition vectors for the transition states are obtained at 1178i and 1114i cm^{-1} for TS5 and TS6, respectively. The calculated barrier heights for hydrogen abstraction by OH

radicals and Cl atoms at M06-2X/6-31+G(d,p) level are found to be 1.61 and 2.02 kcal mol^{-1}, respectively. Table 5.2.6 provided the rate coefficient values for reaction channels (5.2.5 and 5.2.6) calculated at M06-2X/6-31+G(d,p) level within a temperature range of 250–450 K. At 298 K, our calculated rate constant (2.03×10^{-14} cm^3 $molecule^{-1}$ s^{-1}) is found to be almost same as experimental value of $(2.04\pm0.32)\times10^{-14}$ cm^3 $molecule^{-1}$ s^{-1} reported by Chen *et al.*[43] for the n-$C_3F_7C(O)H$ species. Thus, it reflects that the presence of n-C_3F_7 or i-C_3F_7 group do not have too much affect on the rate of hydrogen abstraction by OH radicals. The rate constant for H atom abstraction reaction of i-$C_3F_7OC(O)H$ by Cl atoms as given by reaction (5.2.6) are calculated as k_{TS6} $=3.03\times10^{-14}$ cm^3 $molecule^{-1}$ s^{-1} at M06-2X/6-31+G(d,p) level which is in a reasonable agreement with experimental value of $(1.6\pm0.7)\times10^{-14}$ cm^3 $molecule^{-1}$ s^{-1} by Andersen *et al.* [42] at 298 K. The OH-driven atmospheric lifetime of i-$C_3F_7OC(O)H$ are computed to be 3.01 years. The temperature variations of k_{TS5} and k_{TS6} results obtained at M06-2X/6-31+G(d,p) level are shown in Figure 5.2.5.

Table 5.2.6 Rate coefficient values (in cm^3 $molecule^{-1}$ s^{-1}) for reactions R5 and R6 using M06-2X/6-31+G(d,p) results.

Temp (K)	**M06-2X/6-31+G(d,p)**	
	$\mathbf{k_{TS5}}$	$\mathbf{k_{TS6}}$
250	1.78×10^{-14}	2.13×10^{-14}
298	2.03×10^{-14}	3.03×10^{-14}
300	2.05×10^{-14}	3.06×10^{-14}
350	2.38×10^{-14}	4.19×10^{-14}
400	2.75×10^{-14}	5.52×10^{-14}
450	3.18×10^{-14}	6.99×10^{-14}

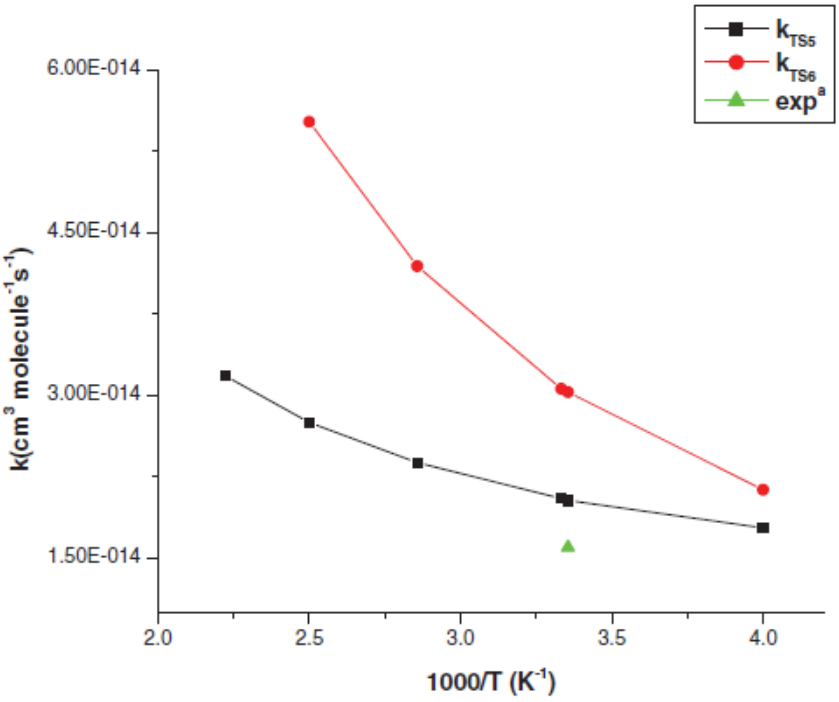

Figure 5.2.5 Rate constants for hydrogen abstraction reactions of i-$C_3F_7OC(O)H$ + OH/Cl reactions with experimental data. [a]Ref. [42]

5.2.4 SALIENT OBSERVATIONS

In this section, we have studied the atmospheric chemistry and reaction kinetics of the H-abstraction reaction of i-$C_3F_7OCH_3$ with OH radicals using M06-2X/6-31+G(d,p) level of theory. The study reveals the following observations:

1. The reaction with OH radicals follows an indirect path via the pre- and post-reaction complexes formation.
2. Two transition states have been located for the titled reaction. The barrier heights for H-abstraction by OH radicals are resulted as 2.13 and 3.46 kcal mol^{-1}, respectively.
3. The thermal rate constant for the H atom abstraction of i-$C_3F_7OCH_3$ by OH radicals is found to be 2.36×10^{-14}cm^{3}molecule^{-1}s^{-1} at 298 K which is in reasonable agreement with experimental data. The $\Delta_fH°_{298}$ for i-$C_3F_7OCH_3$ and i-$C_3F_7OC^{\bullet}H_2$ species calculated from M06-2X/6-31+G(d,p) results are -414.67

and -365.19 kcal mol^{-1}, respectively. The $D°_{298}$ value obtained for the C–H bond in i-$C_3F_7OCH_3$ amount to 101.63 kcal mol^{-1}.

4. The sole atmospheric fate for thermal decomposition of i-$C_3F_7OCH_2O^{\bullet}$ radical is the reaction with O_2 that occurs with the lowest barrier height.
5. The kinetics for OH and Cl-initated hydrogen abstraction reaction for isofluoro-propyl formate i-$C_3F_7OC(O)H$ are also studied and rate constant for OH reactions are reported for the first time.
6. The atmospheric lifetimes for i-HFE-7000 and i-$C_3F_7OC(O)H$ are estimated to be 3.19 and 3.01 years, respectively.

BIBLIOGRAPHY

[1] Sekiya, A. and Misaki, S. The potential of hydrofluoroethers to replace CFCs, HCFCs and PFCs. *Journal of Fluorine Chemistry*, 101(2):215-221, 2000.

[2] Powell, R. L. CFC phase-out: have we met the challenge? *Journal of Fluorine Chemistry*, 114(2):237-250, 2002.

[3] Imasu, R., Suga, A. and Matsuno, T. Radiative effects and halocarbon global warming potentials of replacement compounds for chlorofluorocarbons. *Journal of the Meteorological Society of Japan. Ser. II*, 73(6):1123-1136, 1995.

[4] Blowers, P., Tetrault, K. F. and Trujillo-Morehead, Y. Global warming potential predictions for hydrofluoroethers with two carbon atoms. *Theoretical Chemistry Accounts*, 119(4):369-381, 2008.

[5] Blanco, M. B., Bejan, I., Barnes, I., Wiesen, P. and Teruel, M. A. Atmospheric photooxidation of fluoroacetates as a source of fluorocarboxylic acids. *Environmental Science and Technology*, 44(7):2354-2359, 2010.

[6] Bravo, I., Díaz-de-Mera, Y., Aranda, A., Moreno, E., Nutt, D. R. and Marston, G. Radiative efficiencies for fluorinated esters: indirect global warming potentials of hydrofluoroethers. *Physical Chemistry Chemical Physics*, 13(38):17185-17193, 2011.

[7] Ninomiya, Y., Kawasaki, M., Guschin, A., Molina, L. T., Molina, M. J., and Wallington, T. J. Atmospheric chemistry of n-$C_3F_7OCH_3$: Reaction with OH radicals and Cl atoms and atmospheric fate of n-$C_3F_7OCH_2O(\bullet)$ radicals. *Environmental Science and Technology*, 34(14):2973-2978, 2000.

[8] Oyaro, N., Sellevåg, S. R. and Nielsen, C. J. Study of the OH and Cl-initiated oxidation, IR absorption cross-section, radiative forcing, and global warming potential of four C4-hydrofluoroethers. *Environmental Science and Technology*, 38(21):5567-5576, 2004.

[9] Thomsen, D. L., Andersen, V. F., Nielsen, O. J. and Wallington, T. J. Atmospheric chemistry of $C_2F_5CH_2OCH_3$ (HFE-365mcf). *Physical Chemistry Chemical Physics*, 13(7):2758-2764, 2011.

[10] Urata, S., Takada, A., Uchimaru, T. and Chandra, A. K. Rate constants estimation for the reaction of hydrofluorocarbons and hydrofluoroethers with OH radicals. *Chemical Physics Letters*, 368(1), 215-223, 2003.

[11] Dalmasso, P. R., Taccone, R. A., Nieto, J. D., Cometto, P. M., Cobos, C. J. and Lane, S. I. Reactivity of hydrohaloethers with OH radicals and chlorine atoms: Correlation with molecular properties. *Atmospheric Environment*, 91:104-109, 2014.

[12] Chandra, A. K. and Uchimaru, T. The C–H bond dissociation enthalpies of haloethers and its correlation with the activation energies for hydrogen abstraction by OH radical: A DFT study. *Chemical Physics Letters*, 334(1):200-206, 2001.

[13] Frisch, M.J., Trucks, G.W., Schlegel, H.B., Scuseria, G.E., Robb, M.A., Cheeseman, J.R., Scalmani, G., Barone, V., Mennucci, B., Petersson, G.A., Nakatsuji, H., Caricato, M., Li, X., Hratchian, H.P., Izmaylov, A.F., Bloino, J., Zheng, G., Sonnenberg, J.L., Hada, M., Ehara, M., Toyota, K., Fukuda, R., Hasegawa, J., Ishida, M., Nakajima, T., Honda, Y., Kitao, O., Nakai, H., Vreven, T., Montgomery, J.A., Jr., Peralta, J.E., Ogliaro, F., Bearpark, M., Heyd, J.J., Brothers, E., Kudin, K.N., Staroverov, V.N., Kobayashi, R., Normand, J., Raghavachari, K., Rendell, A., Burant, J.C., Iyengar, S.S., Tomasi, J., Cossi, M., Rega, N., Millam, J.M., Klene, M., Knox, J.E., Cross, J.B., Bakken, V., Adamo, C., Jaramillo, J., Gomperts, R., Stratmann, R.E., Yazyev, O., Austin, A.J., Cammi, R., Pomelli, C., Ochterski, J.W., Martin, R.L., Morokuma, K., Zakrzewski, V.G., Voth, G.A., Salvador, P., Dannenberg, J.J., Dapprich, S., Daniels, A.D., Farkas, Ö., Foresman, J.B., Ortiz, J.V., Cioslowski, J. and Fox, D.J. Gaussian 09, Revision A.1, Gaussian, Inc., Wallingford CT, 2009.

[14] Zhao, Y. and Truhlar, D. G. The M06 suite of density functionals for main group thermochemistry, thermochemical kinetics, noncovalent interactions, excited states, and transition elements: two new functionals and systematic testing of four M06-class functionals and 12 other functionals. *Theoretical*

Chemistry Accounts: Theory, Computation, and Modeling (Theoretica Chimica Acta), 120(1):215-241, 2008.

[15] Beste, A. and Buchanan III, A. C. Substituent effects on the reaction rates of hydrogen abstraction in the pyrolysis of phenethyl phenyl ethers. *Energy and Fuels*, 24(5):2857-2867, 2010.

[16] Mishra, B. K., Lily, M., Chandra, A. K. and Deka, R. C. Theoretical studies on atmospheric chemistry of HFE-347mcc3: reactions with OH radicals and Cl atoms. *Journal of Physical Organic Chemistry*, 27(10):811-817, 2014.

[17] Lily, M., Mishra, B. K., and Chandra, A. K. Kinetics, mechanism and thermochemistry of the gas phase reactions of $CF_3CH_2OCH_2CF_3$ with OH radicals: A theoretical study. *Journal of Fluorine Chemistry*, 161:51-59, 2014.

[18] Dinadayalane, T. C., Paytakov, G. and Leszczynski, J. Computational study on C− H… π interactions of acetylene with benzene, 1, 3, 5-trifluorobenzene and coronene. *Journal of Molecular Modeling*, 19(7):2855-2864, 2013.

[19] Sandhiya, L., Kolandaivel, P. and Senthilkumar, K. Theoretical studies on the reaction mechanism and kinetics of the atmospheric reactions of 1, 4-thioxane with OH radical. *Structural Chemistry*, 23(5):1475-1488, 2012.

[20] Mandal, D., Sahu, C., Bagchi, S. and Das, A. K. Kinetics and mechanism of the tropospheric oxidation of vinyl acetate initiated by OH radical: A theoretical study. *The Journal of Physical Chemistry A*, 117(18):3739-3750, 2013.

[21] Chandra, A. K. Theoretical studies on the kinetics and mechanism of the gas-phase reactions of CHF_2OCHF_2 with OH radicals. *Journal of Molecular Modeling*, 18(9):4239-4247, 2012.

[22] Devi, K. J. and Chandra, A. K. Theoretical investigation of the gas-phase reactions of $(CF_3)_2CHOCH_3$ with OH radical. *Chemical Physics Letters*, 502(1):23-28, 2011.

[23] Gonzalez, C. and Schlegel, H. B. An improved algorithm for reaction path following. *The Journal of Chemical Physics*, 90(4):2154-2161, 1989.

[24] Hammond, G. S. A correlation of reaction rates. *Journal of the American Chemical Society*, 77(2):334-338, 1955.

[25] Beste, A., and Buchanan, A. C. Kinetic simulation of the thermal degradation of phenethyl phenyl ether, a model compound for the β-O-4 linkage in lignin. *Chemical Physics Letters*, 550:19-24, 2012.

[26] Younker, J. M., Beste, A. and Buchanan, A. C. Computational study of bond dissociation enthalpies for lignin model compounds: β-5 arylcoumaran. *Chemical Physics Letters*, 545:100-106, 2012.

[27] Csontos, J., Rolik, Z., Das, S., and Kállay, M. High-accuracy thermochemistry of atmospherically important fluorinated and chlorinated methane derivatives. *The Journal of Physical Chemistry A*, 114(50):13093-13103, 2010.

[28] Kondo, S., Takahashi, A., Tokuhashi, K., Sekiya, A., Yamada, Y. and Saito, K. Theoretical calculation of heat of formation for a number of moderate sized fluorinated compounds. *Journal of Fluorine Chemistry*, 117(1):47-53, 2002.

[29] Laidler, K.J. *Chemical kinetics*, Pearson Education, New Delhi, 2004.

[30] Brown, R. L. A method of calculating tunneling corrections for Eckart potential barriers. *Journal of Research of the National Bureau of Standards*, 86:357-359, 1981.

[31] Xiao, R., Noerpel, M., Ling Luk, H., Wei, Z. and Spinney, R. Thermodynamic and kinetic study of ibuprofen with hydroxyl radical: a density functional theory approach. *International Journal of Quantum Chemistry*, 114(1):74-83, 2014.

[32] Chuang, Y. Y. and Truhlar, D. G. Statistical thermodynamics of bond torsional modes. *The Journal of Chemical Physics*, 112(3):1221-1228, 2000.

[33] Singleton, D. L., and Cvetanovic, R. J. Temperature dependence of the reaction of oxygen atoms with olefins. *Journal of the American Chemical Society*, 98(22):6812-6819, 1976.

[34] Blanco, M. B., Rivela, C. and Teruel, M. A. Tropospheric degradation of 2, 2, 2 trifluoroethyl butyrate: Kinetic study of their reactions with OH radicals and Cl atoms at 298K. *Chemical Physics Letters*, 578:33-37, 2013.

[35] Spicer, C. W., Chapman, E. G., Finlayson-Pitts, B. J., Plastridge, R. A., Hubbe, J. M., Fast, J. D. and Berkowitz, C. M. Unexpectedly high concentrations of molecular chlorine in coastal air. *Nature*, 394(6691):353-356, 1998.

[36] Spivakovsky, C. M., Logan, J. A., Montzka, S. A., Balkanski, Y. J., Foreman-Fowler, M., Jones, D. B. A., Horowitz, L.W., Fusco, A.C., Brenninkmeijer, C.A.M., Prather, M.J. and Wofsy, S. C. Three-dimensional climatological distribution of tropospheric OH: Update and evaluation. *Journal of Geophysical Research: Atmospheres*, 105(D7):8931-8980, 2000.

[37] Bravo, I., Aranda, A., Hurley, M. D., Marston, G., Nutt, D. R., Shine, K. P., Smit, K. and Wallington, T. J. Infrared absorption spectra, radiative efficiencies, and global warming potentials of perfluorocarbons: Comparison between experiment and theory. *Journal of Geophysical Research: Atmospheres*, 115(D24):1-12, 2010.

[38] Tokuhashi, K., Takahashi, A., Kaise, M., Kondo, S., Sekiya, A., Yamashita, S., and Ito, H. Rate constants for the reactions of OH radicals with $CH_3OCF_2CF_3$, $CH_3OCF_2CF_2CF_3$, and $CH_3OCF(CF_3)_2$. *International Journal of Chemical Kinetics*, 31(12):846-853, 1999.

[39] Díaz-de-Mera, Y., Aranda, A., Bravo, I., Rodríguez, D., Rodríguez, A. and Moreno, E. (2008). Atmospheric chemistry of HFE-7000 ($CF_3CF_2CF_2OCH_3$) and 2, 2, 3, 3, 4, 4, 4-heptafluoro-1-butanol ($CF_3CF_2CF_2CH_2OH$): kinetic rate coefficients and temperature dependence of reactions with chlorine atoms. *Environmental Science and Pollution Research*, 15(7):584, 2008.

[40] Bravo, I., Díaz-de-Mera, Y., Aranda, A., Smith, K., Shine, K. P., and Marston, G. Atmospheric chemistry of $C_4F_9OC_2H_5$ (HFE-7200), $C_4F_9OCH_3$ (HFE-7100), $C_3F_7OCH_3$ (HFE-7000) and $C_3F_7CH_2OH$: temperature dependence of the kinetics of their reactions with OH radicals, atmospheric lifetimes and global warming potentials. *Physical Chemistry Chemical Physics*, 12(19):5115-5125, 2010.

[41] Aranda, A., Díaz-de-Mera, Y., Bravo, I., Rodríguez, D., Rodríguez, A. and Martínez, E. (2006). Atmospheric HFEs degradation in the gas phase:

Reactions of HFE-7100 and HFE-7200 with Cl atoms at low temperatures. *Environmental Science and Technology*, 40(19):5971-5976, 2006.

[42] Andersen, L. L., Østerstrøm, F. F., Nielsen, O. J., Andersen, M. P. S. and Wallington, T. J. Atmospheric chemistry of $(CF_3)_2CFOCH_3$. *Chemical Physics Letters*, 607:5-9, 2014.

[43] Chen, L., Kutsuna, S., Tokuhashi, K. and Sekiya, A. Kinetics study of the gas-phase reactions of $C_2F_5OC(O)H$ and n-$C_3F_7OC(O)H$ with OH radicals at 253–328 K. *Chemical Physics Letters*, 400(4):563-568, 2004.

[44] Kondo, S., Takahashi, A., Tokuhashi, K., Sekiya, A., Yamada, Y. and Saito, K. Theoretical calculation of heat of formation for a number of moderate sized fluorinated compounds. *Journal of Fluorine Chemistry*, 117(1):47-53, 2002.

[45] Wallington, T. J., Schneider, W. F., Sehested, J., Bilde, M., Platz, J., Nielsen, O. J., Christensen, L.K., Molina, M.J., Molina L.T. and Wooldridge, P. W. Atmospheric chemistry of HFE-7100 ($C_4F_9OCH_3$): reaction with OH radicals, UV spectra and kinetic data for $C_4F_9OCH_2$(•) and $C_4F_9OCH_2O_2$(•) radicals, and the atmospheric fate of $C_4F_9OCH_2O$(•) radicals. *The Journal of Physical Chemistry A*, 101(44):8264-8274, 1997.

[46] Ninomiya, Y., Kawasaki, M., Guschin, A., Molina, L. T., Molina, M. J. and Wallington, T. J. (2000). Atmospheric chemistry of n-$C_3F_7OCH_3$: Reaction with OH radicals and Cl atoms and atmospheric fate of n-$C_3F_7OCH_2O$(•) radicals. *Environmental Science and Technology*, 34(14):2973-2978, 2000.

[47] Kurylo, M. J., and Orkin, V. L. Determination of atmospheric lifetimes via the measurement of OH radical kinetics. *Chemical Reviews*, 103(12):5049-5076, 2003.

[48] Hodnebrog, Ø., Etminan, M., Fuglestvedt, J. S., Marston, G., Myhre, G., Nielsen, C. J., Keith P. S. and Wallington, T. J. Global warming potentials and radiative efficiencies of halocarbons and related compounds: A comprehensive review. *Reviews of Geophysics*, 51(2):300-378, 2013.